High-performance polyesters from carbon dioxide – novel polyhydroxyarylates from engineered *Cupriavidus necator*

Nils JH Averesch[1,3]*, Vince E Pane[2,3], Frauke Kracke[1], Marika Ziesack[4], Shannon N Nangle[4], Robert W Waymouth[2,3], Craig S Criddle[1,3]

(1) *Department of Civil and Environmental Engineering, Stanford University, CA, USA*
(2) *Department of Chemistry, Stanford University, CA, USA*
(3) *Center for the Utilization of Biological Engineering in Space, CA, USA*
(4) *Wyss Institute for Biologically Inspired Engineering, MA, USA*

* Correspondence: nils.averesch@uq.net.au

Abstract

Synthetic materials are integral components of consumable and durable goods and are indispensable in the modern world. Polyesters are the most versatile bulk- and specialty-polymers but their production is not sustainable and their fate at end-of-life is of great concern. Bioplastics are highly regarded alternatives but often fall behind conventional synthetic plastics due to shortcomings in material properties and commercial competitiveness. This has limited the success of sustainable replacements at global market scale. Enabling production of bioplastics with superior properties from waste-derived feedstocks could change that. To this end, we created a synthetic entry into the metabolic pathway of bio-polyester synthesis of *Cupriavidus necator* H16 by means of heterologous hydroxyacyl-CoA transferase and mutant PHA synthase. The resulting microbial cell factories produced a range of aliphatic and aromatic bio-polyesters and enabled co-polymerization of a range of hydroxy carboxylates, including a hydroxyphenylic and a hydroxyfuranoic acid, for the first time incorporating aromatic rings in the backbone of biological polyesters. These diverse polymers were then characterized in terms of their physical properties. The resulting polymers were structurally analogous to synthetic polyesters like PET, PEF and other polyarylates. In a further advance, the transgenic strain was cultivated in a bio-electrochemical system under autotrophic conditions, enabling synthesis of aromatic bio-polyesters from *in-situ* generated O_2, while assimilating CO_2. Follow-up elementary flux-mode analysis established the feasibility of *de novo* production of twenty different polyesters from five different carbon- and energy-sources. This comprehensive study opens the door to sustainable bio-production of various high-performance thermoplastics and thermosets.

Significance statement

Biomaterials can facilitate the transition of chemical industry to a carbon-neutral and circular economy and prevent the accumulation of greenhouse gases and plastic waste in the natural environment by developing bio-replacements for existing fossil carbon-based plastics along with end-of-life strategies. Accomplished via the genetic engineering of a microbial cell factory that assimilates carbon dioxide, this work demonstrates the first biocatalytic polymerization of aromatic building blocks and their incorporation into the backbone of a bio-polyester. Employing a bio-electrochemical system for cultivation of the microbes, oxyhydrogen is formed and consumed *in-situ*, thus avoiding explosive gas-mixtures. The obtained aromatic polyesters are structural analogs to synthetic bulk- and high-performance polymers such as PET (polyethylene terephthalate) and PEF (polyethylene furanoate).

Highlights

- First demonstration of bio-polyarylates – microbial polyesters with aromatic rings in the backbone
- Production of novel PHAs from CO_2 and H_2+O_2 achieved *in-situ* in a bio-electrochemical system
- Expression-level of PHA synthase and molecular weight of polyesters is inversely correlated
- *In silico* design and pathway analysis of bio-polyesters from low-cost carbon-feedstocks

Keywords

Polyhydroxyalkanoates, aromatic polyesters, bioplastics, C-1 feedstocks, microbial electrosynthesis

Abbreviations

3HP, 3-hydroxypropionic acid; 4HB, 4-hydroxybutyric acid; 5HM2FA, 5-hydroxymethyl-2-furanoic acid; 6HC, 6-hydroxycaproic acid; BES, bio-electrochemical system; BM, biomass; CDW, cell dry weight; DAP diaminopimelate; DSC, differential scanning calorimetry; EMA, elementary flux-mode analysis; GC-MS, gas chromatography–mass spectrometry; GPC, gel permeation chromatography; HA, hydroxy acid; MA, mandelic acid; MES, microbial electrosynthesis; M_n, number-average molecular weight; MSM, mineral salts medium; M_W, weight-average molecular weight; NMR, nuclear magnetic resonance; OD, optical density; PA, phloretic acid; PDI, polydispersity index; PEF, polyethylene furanoate: PET, polyethylene terephthalate; PHA, polyhydroxyalkanoate; PHB, polyhydroxybutyrate; PHBV, polyhydroxybutyrate-co-hydroxyvalerate; PheLA, phenyllactic acid; PLA, polylactic acid; RB, rich broth; rpm, rounds per minute; VFA, volatile fatty acid;

1 Introduction

1.1 Background

Modern society is based upon ever-increasing consumption of energy and material resources, along with ever-increasing emissions of waste and pollutants (1). Greenhouse gases are reaching critical levels, and pollution from fabrication of recalcitrant synthetic materials is ubiquitous and undeniable (2). A lifestyle and an economy dependent upon plastic consumption risks serious harm to the biosphere (3). To ensure a viable planet for generations to come, methods are needed to reduce waste accumulation while embracing readily available and renewable feedstocks (4). While recycling of plastic is necessary for a circular economy, it will not be able to fully prevent unintended release of synthetic materials into the environment (5). This is of particular relevance in single-use applications where the stability of plastics is as unnecessary as problematic (6). While bio-degradable materials derived from renewable feedstocks or from upcycling of existing materials are desirable (7), production from cultivated feedstocks is not necessarily cost effective nor carbon-negative or -neutral (8). An alternative is the utilization of ultra-low-cost (waste) carbon-sources, such as C1-feedstocks, for production of materials can directly mitigate greenhouse gas emissions while avoiding competition with the food-industry (9). Such a strategy also improves commercial competitiveness by decreasing feedstock-cost (10). Especially useful are compounds that can substitute for or directly replace industrial (petrochemistry-based) polymers. Such bio-replacements are attractive because they do not require extensive modifications to the existing infrastructure for processing and manufacturing.

Polyhydroxybutyrate (PHB), a biological thermoplastic polyester, can be produced outgoing from non-edible, waste-derived carbon-sources, such as carbon dioxide or methane, and could be a bio-degradable replacement for synthetic materials (11). To date, however, insufficient material properties (12) and high production-costs (10) have hampered commercialization and widespread adoption by the manufacturing industry. Nevertheless, a multitude of polyhydroxyalkanoates (PHAs) have been generated from alternative co-monomers, enabling tuning of material properties (12). For example, linear short-chain PHAs, have high-strength and -flexibility (13-15), while aromatic groups in the side-chain lead to more amorphic polymers with increased glass-transition and degradation temperatures, conferring wider processing windows (16). For example, polymers of mandelic and phenyllactic acid, poly(mandelite) (17) and poly(phenyllactide) (18), respectively, have been chemically synthesized and characterized. These polymers exhibited properties mimicking those of polystyrene.

To date, all biocatalytically produced aromatic PHAs contain the aromatic ring on a side chain branching off from the polymer backbone (16). Incorporation of aromatic rings into the bio-polyester backbone could vastly alter material properties, conceivably resembling those of synthetic aromatic polyesters, such as e.g., polyethylene terephthalate (PET), polyethylene furanoate (PEF) or even polyarylates. Analogous polyesters that are based on bio-derivable building blocks have been chemically synthesized and characterized, such as co-polymers of glycolic and *para*-hydroxybenzoic acid (19), as well as 3-(*para*-hydroxyphenyl)propionic (phloretic) and 3-(*para*-hydroxyphenyl)acrylic (coumaric) acid (20). These "polyhydroxy*arylates*" exhibit liquid-crystal polymer properties and full biosynthesis of such polymers could open the door to a new realm of renewable materials with superior properties (16).

1.2 Concept

Here microbial production of various bio-polyesters from sustainable feedstocks is explored *in vivo* and *in silico*, using the 'knallgas' bacterium *Cupriavidus necator*. This well-characterized mixotroph can make use of a wide range of carbon- and energy-sources, grows rapidly to high cell density, and is an excellent producer of polyhydroxybutyrate (PHB) (21). As a chemolithoautotroph that utilizes carbon dioxide and oxyhydrogen (22), it has previously been engineered for production of non-natural PHAs, including fatty acid-derived medium chain-length poly(3-hydroxyalkanoate)s and co-polymers of lactic acid (23). Incorporation of exogenously supplied aromatic precursors has also been explored (24).

Specifically, a Δ*phaC1* knock-out mutant of *C. necator* H16 was complemented with the genes coding for a hydroxyacyl-CoA transferase (*pct540* or *hadA* from *Clostridium propionicum* or *Clostridium difficile*, respectively) and a mutant PHA synthase (*phaC1437* from *Pseudomonas* sp. MBEL 6-19), which previously proved useful for production of non-natural PHAs in *E. coli* (25, 26). The second entry into the PHA synthesis of *C. necator* (cf. figure 1) enabled formation of several straight-chain aliphatic and aromatic PHAs, complementing and diversifying natural *poly*(3-hydroxbutyrate) (PHB) production.

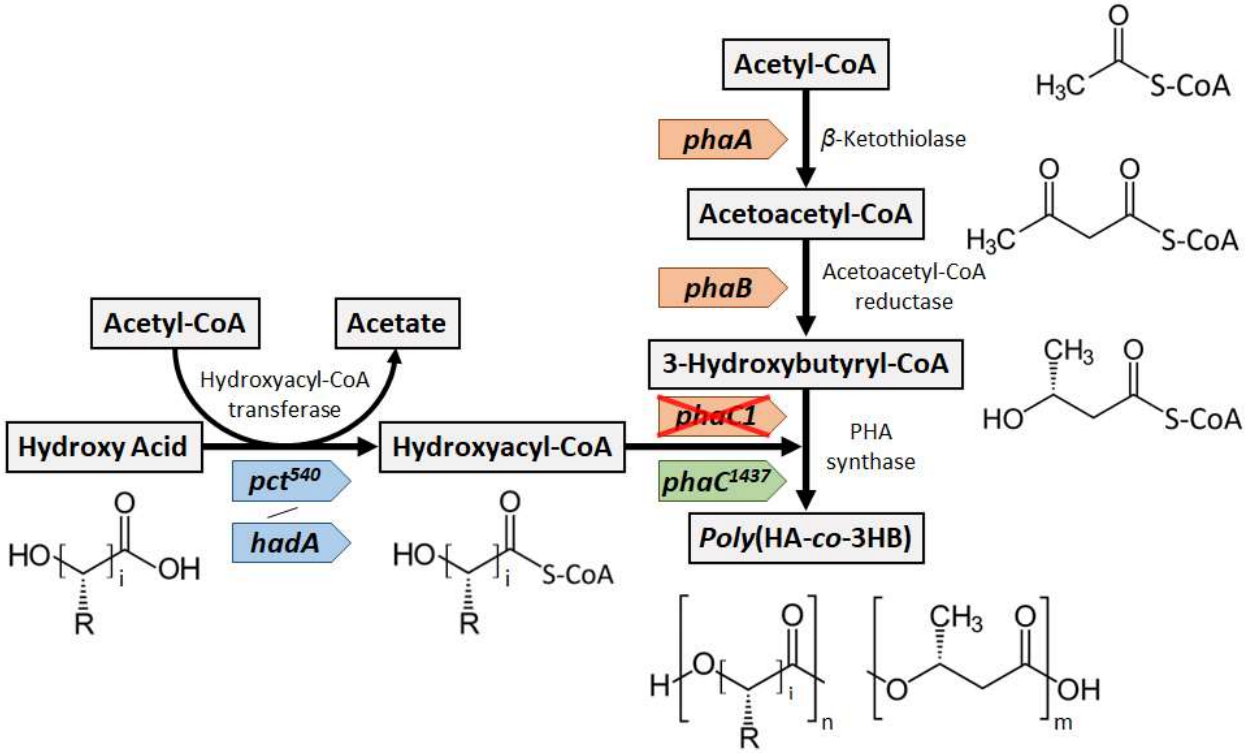

Figure 1: Partial breakdown of metabolic route for biosynthesis of diverse polyhydroxyalkanoates. The non-natural segment (horizontal) provides alternative polymer building-blocks to the endogenous pathway of *poly*(3-hydroxybutyrate) biosynthesis (vertical). Heterologous genes (blue and green) complement the natural biosynthetic route (orange) and mediate the formation of modified bio-polyesters. The heterologous CoA-transferases (*pct540* or *hadA*) were implemented alternatively, while the mutant PHA synthase (*phaC1437*) substituted the natural PHA synthase (*phaC*1). In the generalized chemical structures "R" can assume a proton or a phenolic residue; "i" may reflect any of 1 to 6 carbons, while "m" and "n" indicate the polymeric character of the molecule with uncorrelated statistic distribution of the co-monomers. The hitherto hypothetical bio-polyesters with aromatic rings in the polymer backbone have not been included in the structural depiction.

2 Results and Discussion

2.1 Formation of Non-Natural Polyesters from Exogenous Precursors

Introduction of the heterologous PHA synthase "PhaC1437" into *C. necator* H16 Δ*phaC1* rescued the PHB-negative phenotype of the knock-out mutant. Per-biomass yield was comparable to the wild-type (≈ 60% $w_{PHA}/w_{BIOMASS}$, data not shown); notably, bio-polyesters were formed independent of induction of expression of the heterologous genes under control of P_{BAD}. Nuclear magnetic resonance (NMR) spectroscopy revealed that these were mainly composed of 3-hydroxybutyrate (3HB). When expression of the heterologous genes was induced, the polymers also contained small fractions of other (natural) hydroxy acids, depending on the employed CoA-transferase (see SI 1, figure S8 and S9).

Several rounds of feeding experiments with various hydroxy carbonic acids were conducted using mutant strains and the wild-type in batch shake-flask cultures. The composition of the obtained polyesters as well as the respective fraction of non-natural monomers in the co-polymer were determined by means of ^{1}H-NMR spectroscopy, which was in certain cases complemented with ^{13}C-NMR spectroscopy (cf. SI 1, table S2), as well as gas-chromatography coupled mass-spectroscopy (GC-MS). Table 1 summarizes the range and concentration of exogenously provided precursors, the identity of different polyesters formed, and the ratios of the fraction of non-natural monomer incorporated in the polymer.

Table 1: Polymers obtained from feeding experiments of *C. necator* H16 (wild-type and engineered strains) with precursors and fraction of non-natural monomer in the obtained co-polyester. Ratios are based on ^{1}H-NMR spectroscopy. The composition as per GC-MS analysis can be found in SI 1 (table S1).

Precursor / Concentration		Strain / co-polymer & ratio of repeat units		
		H16 (*wild-type*)	H16 Δ*phaC1 pct540 phaC1437*	H16 Δ*phaC1 hadA phaC1437*
–	N/A	*P*3HB[a] #1	*P*3HB[b] #2	*P*3HB[c] #3
glycolic acid	20 mM	*P*3HB[a]	*P*3HB[b]	*P*3HB[c]
D-lactic acid	20 mM	*P*3HB[a]	*P*3HB[b]	*P*3HB[c]
3-hydroxypropionic acid	20 mM	*P*3HB[a]	*P*(3HB-*co*-3HP) ≈ 100:12	*P*(3HB-co-3HP) ≈ 100:1
4-hydroxybutyric acid	20 mM	*P*(3HB-*co*-4HB) ≈ 100:9[$]	*P*(3HB-*co*-4HB) ≈ 1:1	*P*(3HB-*co*-4HB) ≈ 10:1
6-hydroxycaproic acid	< 10 mM*	*P*(3HB-*co*-4HB) ≈ 100:13	*P*(3HB-*co*-4HB-*co*-6HC) ≈ 100:13:8	*P*(3HB-*co*-4HB-*co*-6HC) ≈ 100:5:2
2-hydroxy-4-phenylbutyric acid	10 mM	n.d.	*P*3HB	*P*(3HB-*co*-2H4PheB) ≈ 20:1
D-phenyllactic acid	10 mM	n.d.	*P*3HB	*P*(3HB-*co*-PheLA) ≈ 2:1
mandelic acid	5 mM	n.d.	*P*3HB	*P*(3HB-*co*-MA) ≈ 4:1
phloretic acid	5 mM	n.d.	*P*3HB	*P*(3HB-*co*-PA) ≈ 100:1
5-hydroxymethyl-2-furanoic acid	5 mM	n.d.	*P*3HB	*P*(3HB-*co*-5HM2FA) ≈ 300:1

* approx. 10 mM supplied (above solubility limit); Abbreviations: n.d. = not determined, 3HP = 3-hyroxypropionate, 3HB = 3-hydroxybutyrate, 4HB = 4-hydroxybutyrate, 6HC = 6-hydroxycaproate, 2H4PheB = 2-hydroxy-4-phenylbutyrate, PheLA = phenyllactate, MA = mandelate, PA = phloretate, 5HM2FA = 5-hydroxymethyl-2-furanoic acid, xHA = indeterminate hydroxycarbonate; [a] natural PHB, [b,c] PHB with minor fraction of indeterminate hydroxycarbonate of natural origin (see figure S8 and S9).

Throughout the batch cultivations, which were conducted with fructose as substrate for experimental simplicity, some of the polymer-precursors appeared to exhibit toxicity, which dictated the maximum employable concentrations, as per Table 1. In particular, hydroxypropionic acids affected the growth rate negatively (data not shown). While not toxic, poor solubility of 6-hydroxycaproic acid (< 10 mM) limited the final concentration of the ω-fatty acid in the growth medium. The aromatic hydroxy acids also exhibited significant toxicity, esp. 2-hydroxy-4-phenylbutyric (2H4PheB) and mandelic acid (MA), which could only be supplied at 10 mM and 5 mM, respectively, to avoid complete inhibition of growth.

Aromatic hydroxy acids were polymerized only by the transgenic variant of *C. necator* H16 carrying *hadA* and *phaC1437*. Most significantly, the *para*-hydroxyphenyl compound 'phloretic acid' (PA) as well as the hydroxyfuranoic compound 5-hydroxymethyl-2-furanoic acid (5HM2FA) were successfully co-polymerized with 3HB, forming *P*(3HB-*co*-PA) and *P*(3HB-*co*-5HM2FA), respectively (figure 2G and 2H). Although the polymers obtained only contained small fractions of the aromatic compounds, no higher than 1%, this is the first-time that incorporation of aromatic rings into the backbone of biological polyesters has been demonstrated, paving the way to a new class of bio-available materials: the obtained co-polymers have structural analogy with synthetic plastics like polyethylene terephthalate (PET) and polyethylene furanoate (PEF) (27), bringing the biocatalytic synthesis of poly(hydroxy)arylates into reach (19, 20).

PHAs with significant aromatics content were obtained from arylaliphatic / arylalkyl hydroxy acids, although incorporation ratios differed depending on the precursor: while external supply of 2H4PheB yielded a co-polymer with a fraction of the aromatic monomer that was roughly one order of magnitude lower than the main (3HB) constituent (figure 2D), incorporation of phenyllactic acid (PheLA) yielded a PHA containing ten-times the fraction (a third of the polymer) of aromatic repeat-units (figure 2E). This led to drastically changed polymer properties, including reduced melting point and increased solubility (e.g., readily soluble in acetone). The dry polymer appeared ductile at room temperature. The polyester obtained with MA as co-substrate (figure 2F) had about half the aromatics content compared to the PheLA-derived co-polymer, which correlated with the lower concentration of precursor supplied.

No co-polymers containing glycolic and lactic acid were obtained from any of the strains. Volatile fatty acids (VFAs) are known to be good substrates for *C. necator* (28-30), and it is likely that these short organic acids were catabolized before they could be polymerized. For a similar reason (31), also the incorporation of 3-hydroxypropionic acid (3HP) was low – nevertheless, the triplet resonance at 4.33 ppm in the ^{1}H-NMR spectra (figure 2A), which is indicative of the C3-methylene, was in good accordance with literature (32). Likewise, incorporation of 4-hydroxybutyric and 6-hydroxyhexanoic acid was identified by shifts of 4.11 and 4.07 ppm (figure 2B and 2C as well as S6 and S7), representative of the protons on the ω-carbon of the originating hydroxy acid, respectively. Incorporation-level of 4-hydroxybutyric acid (4HB) by the engineered strain that carried *hadA* (and *phaC1437*) vs. by the wild-type was similar (≈ 10%). This indicates that the natural PHA synthase (*phaC1*) is promiscuous enough to polymerize the non-natural monomer

while *phaC1437* offers no significant advantage for formation of poly(4HB). Consequentially also a native CoA transferase must exist that accepts 4HB as a substrate at least as well as *hadA*; the respective function is likely provided by the acetate CoA-transferase 'YdiF' (*pct*), as previously reported (33).

Contrarily, the strain carrying *pct540 (*and *phaC1437*) formed a co-polymer with a high fraction of 4HB (approx. 66% as per ^{1}H-NMR, figure 2B). Further analytics (see SI 1, ^{13}C-NMR in figure S11 and GPC plot in figure S27) indicated that the polyester obtained was a block-co-polymer (34). Throughout the course of the cultivation, it was further noted that induction of expression of the heterologous enzymes led to considerably reduced growth of the strain compared to the wild-type or the other transgenic mutant (figures S1 and S2). Retardation of growth correlated with the onset of expression (figures S3 and S4); fructose consumption also came to a halt at that point. Altogether, it appears that severe enzyme toxicity, a known problem of heterologous propionyl-CoA transferases (26), stalled metabolic activity. This would also have halted conversion of acetyl-CoA to 3-hydroxybutyryl-CoA, indicating that the high 4HB content of the PHA produced by the *pct540* strain is likely a result of that effect, rather than the metabolic function(s) of heterologous enzyme(s). This hypothesis can also explain block-co-polymer synthesis: while in early stage (pre-induction) mostly natural poly(3HB) synthesis was active, in the final stage (after induction), pure catalysis would have taken place, with sole addition of exogenous 4HB to the still growing polymer chain. As a measure for the polymer's heterogeneity (varying length/mass of differently composed chains), the comparatively high co-polymer PDI of ≈3 (table S2) supports this interpretation (35).

With externally supplied 6-hydroxycaproic acid (6HC) both engineered strains as well as the wild-type formed non-natural PHAs: while the wild-type produced co-polymers containing 4HB, the PHA derived from the engineered strains contained both 4HB and 6HC (figure 2C). In all cases the presence of the 4HB repeat-units is attributed to the original C6 ω-fatty acid undergoing β-oxidation down to a C4 ω-fatty acid before being incorporated into the polymer. While in the wild-type all of the present 6HC was degraded, in the transgenic strains the heterologous enzymes apparently prevented this, likely through accelerated kinetics: high abundance of the mutant PHA synthase, in concert with the over-expressed CoA transferase was probably able to partially outcompete β-oxidation.

A

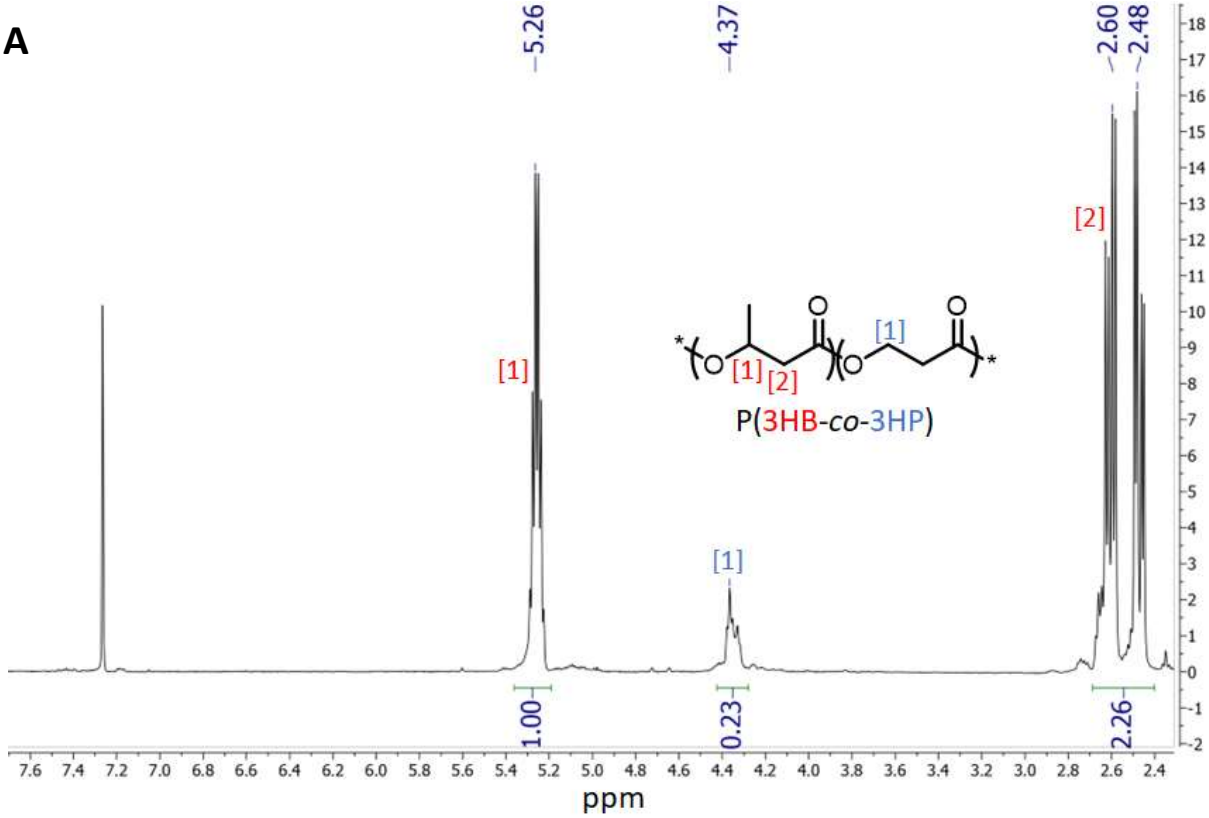
5.26
4.37
2.60
2.48
[1]
[2]
[1]
[1]
[2]
[1]
P(3HB-co-3HP)
1.00
0.23
2.26
ppm

B

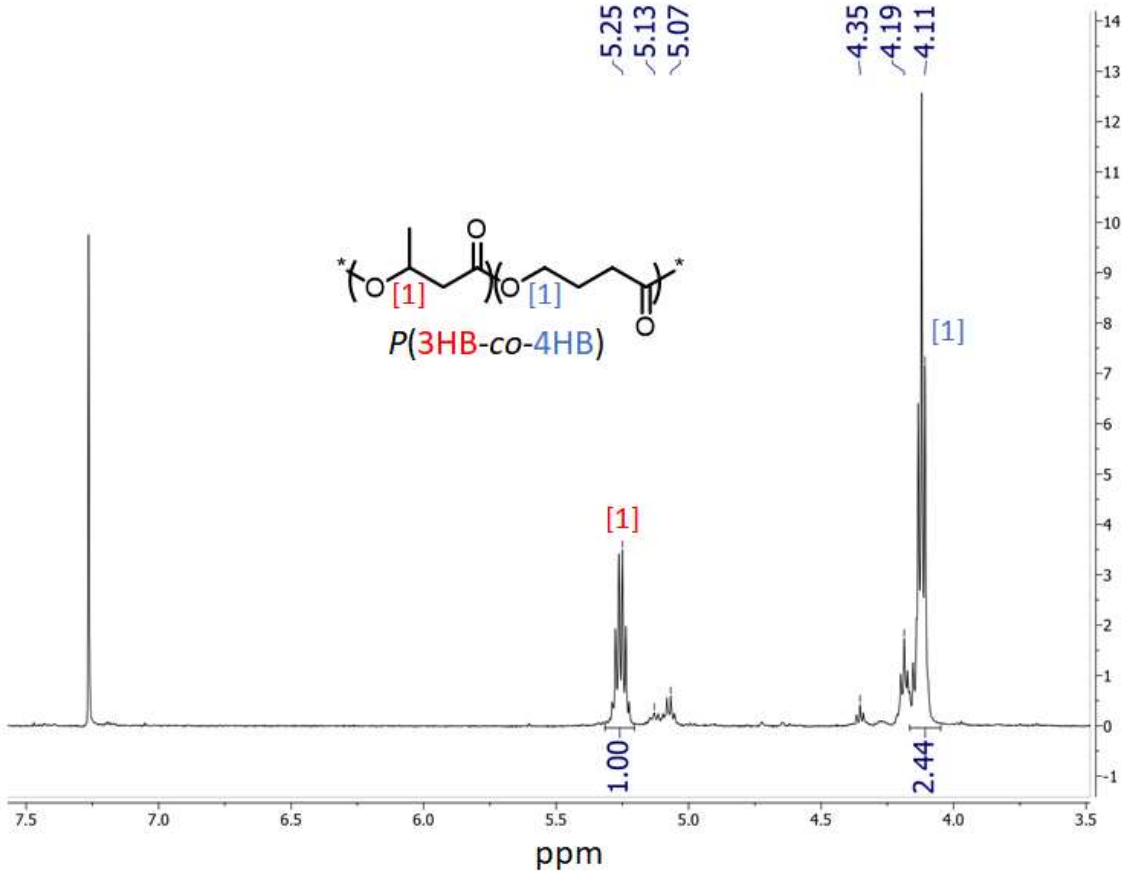
5.25
5.13
5.07
4.35
4.19
4.11
[1]
[1]
[1]
[1]
P(3HB-co-4HB)
1.00
2.44
ppm

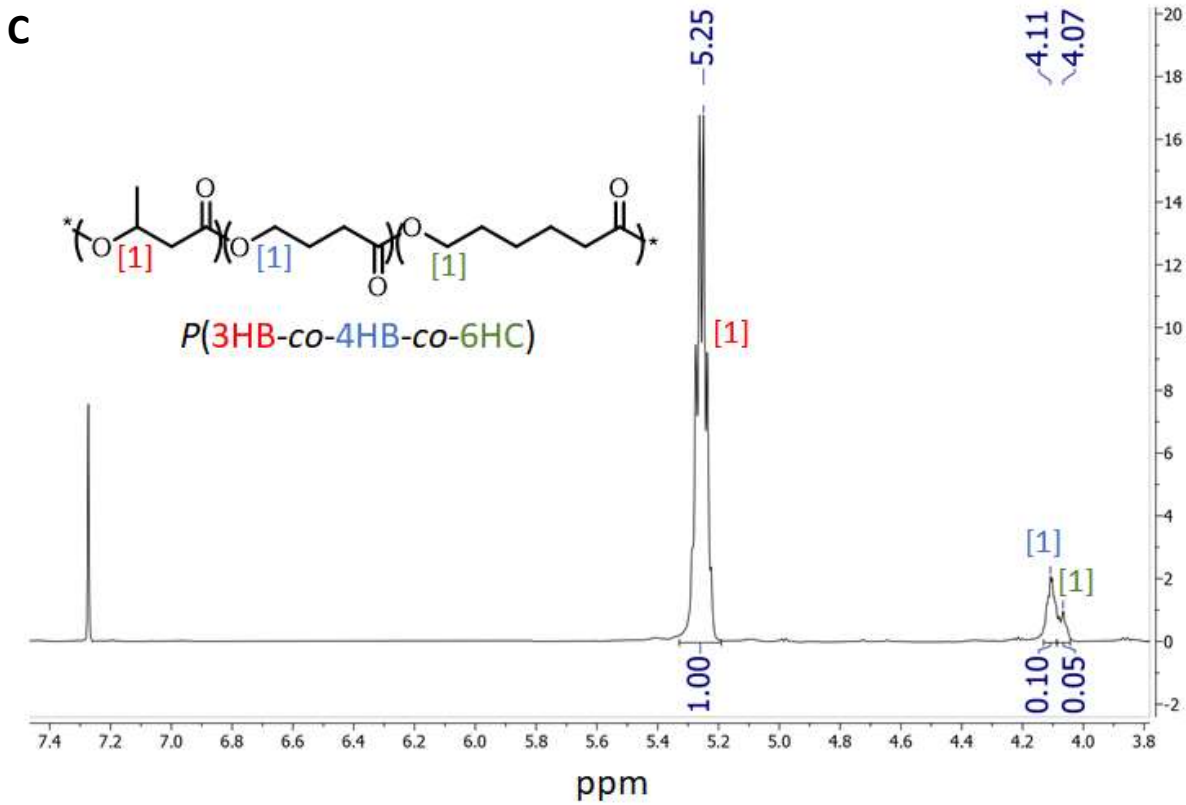
C
5.25
4.11
4.07
[1]
[1]
[1]
[1]
[1]
[1]
P(3HB-co-4HB-co-6HC)
1.00
0.10
0.05
ppm

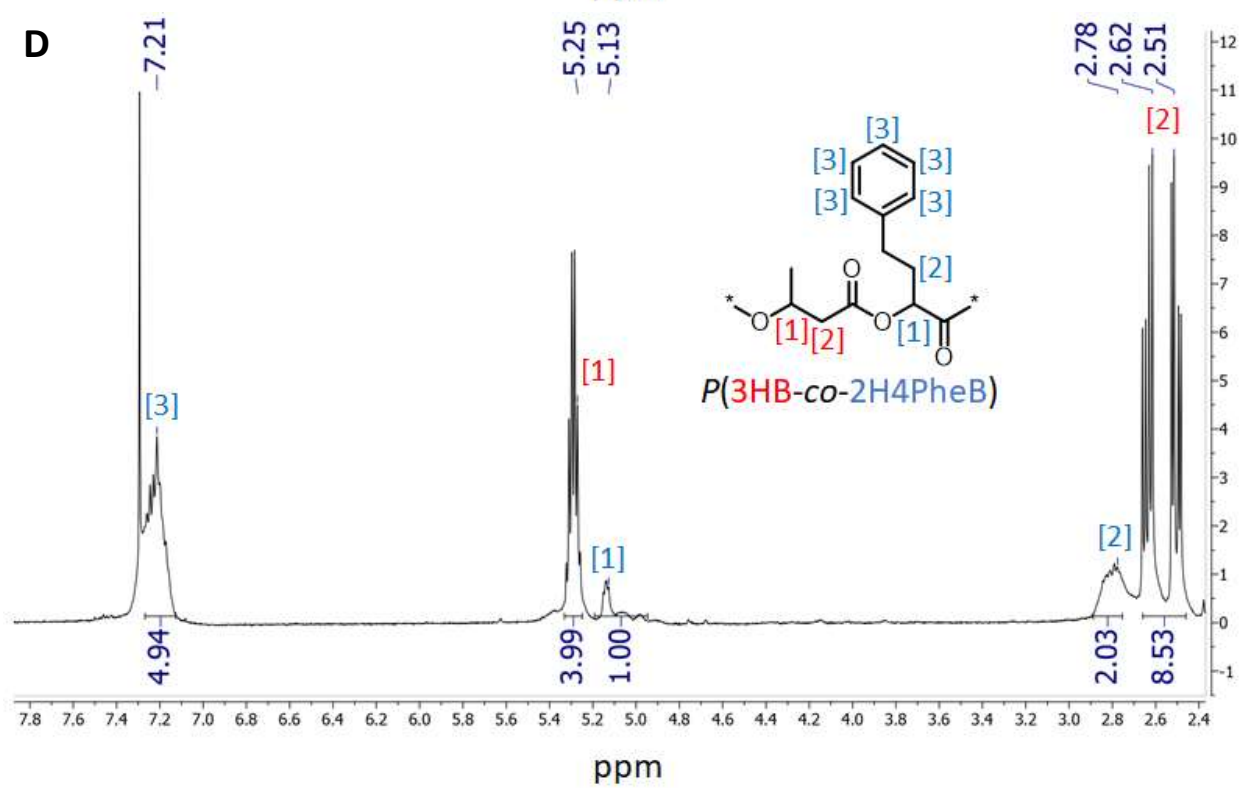
D
7.21
5.25
5.13
2.78
2.62
2.51
[3]
[1]
[1]
[2]
[2]
[3]
[3]
[3]
[3]
[3]
[2]
[1]
[2]
[1]
P(3HB-co-2H4PheB)
4.94
3.99
1.00
2.03
8.53
ppm

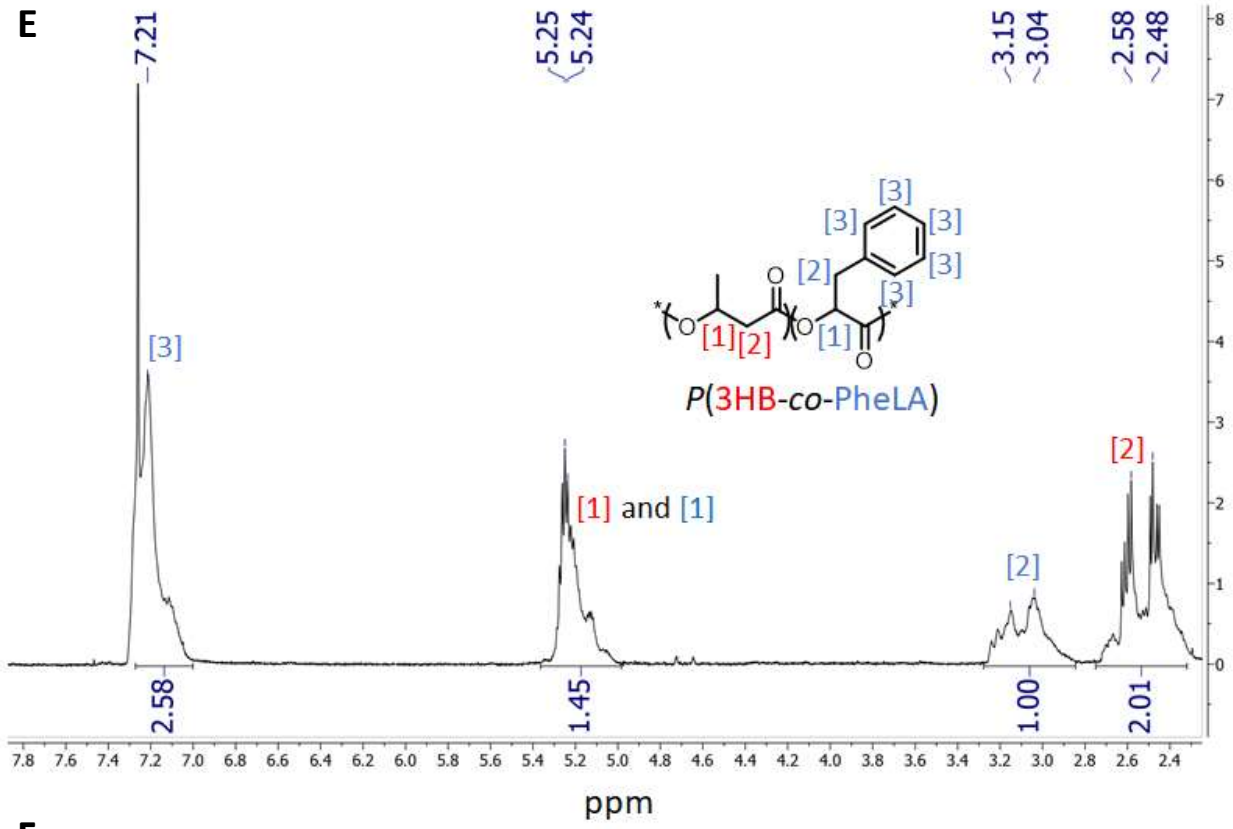
E
7.21
5.25
5.24
3.15
3.04
2.58
2.48
[3]
[1] and [1]
[2]
[2]
P(3HB-co-PheLA)
2.58
1.45
1.00
2.01
ppm

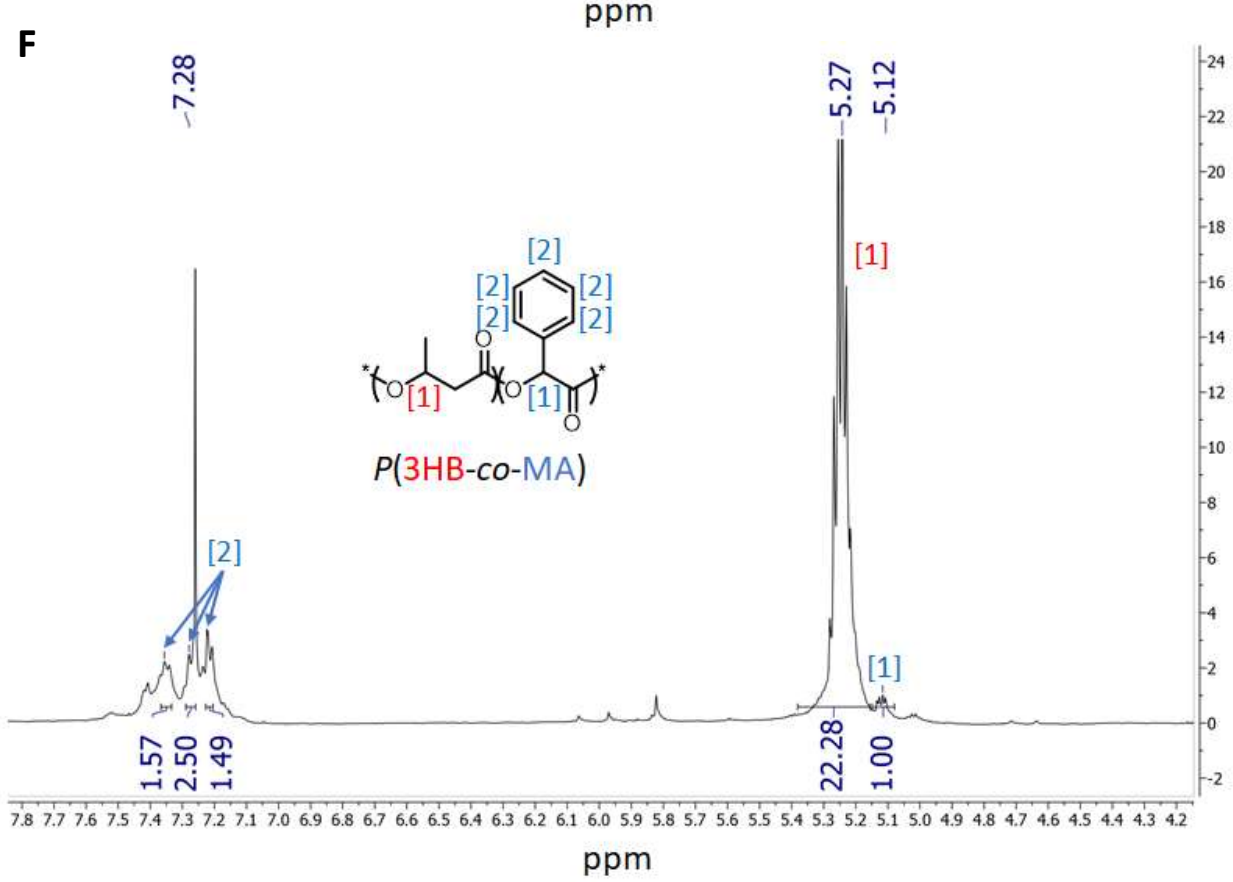
F
7.28
5.27
5.12
[1]
[2]
[2]
[1]
P(3HB-co-MA)
1.57
2.50
1.49
22.28
1.00
ppm

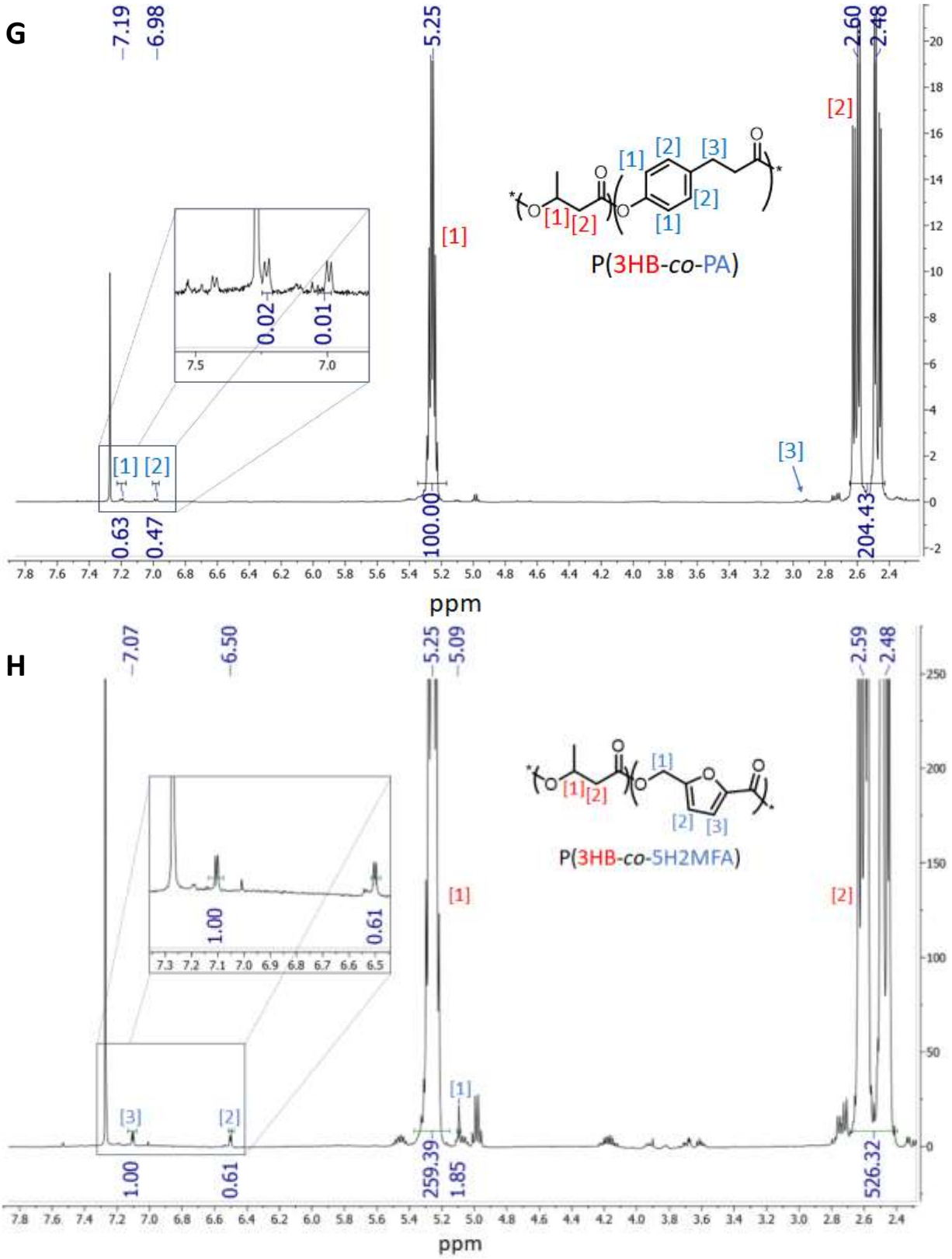

Figure 2: ^{1}H-NMR spectra of *P*(3HB-*co*-3HP) and *P*(3HB-*co*-4HB) produced by *C. necator* H16 Δ*phaC1* pCM66Tp$_{BAD}$:*pct540-phaC1437* (A and B) as well as *P*(3HB-*co*-4HB-*co*-6HC), *P*(3HB-*co*-2H4PheB), *P*(3HB-*co*-PheLA),

***P*(3HB-*co*-MA), *P*(3HB-*co*-PA) and *P*(3HB-*co*-5HM2FA) produced by *C. necator* H16 Δ*phaC1* pCM66Tp$_{BAD}$:*hadA*-*phaC1437* (C to H). Areas below the peaks, weighed by the number of protons they represent, are indicative for the fractions of the respective repeat units. (A): In addition to the 3HB sextet resonance at 5.25 ppm, a triplet resonance at 4.37 ppm shows that the C3-methylene of the 3HP repeat is present, indicating incorporation of 3HP into the polymer. (B): In addition to the 3HB sextet resonance at 5.25 ppm, a triplet resonance at 4.11 ppm shows that the C4-methylene of the 4HB repeat is present, indicating incorporation of 4HB into the polymer. The large fraction of 4HB causes multiple 3HB signals because of different possible orders in the polymer (e.g., -3HB-3HB-4HB-, -4HB-3HB-4HB-, -4HB-3HB-3HB-, -3HB-4HB-3HB-). (C): In addition to the 3HB sextet resonance at 5.25 ppm and 4HB triplet resonance at 4.11 ppm, a triplet resonance at 4.07 ppm shows that the C6-methylene of the 6HC repeat is present, indicating incorporation of 6HC into the polymer. (D): In addition to the 3HB sextet resonance at 5.25 ppm, a triplet resonance at 5.13 ppm shows that the C2-methine of the 2H4PheB repeat is present. The broad aromatic multiplet resonance at 7.21 ppm is also indicative of 2H4PheB. (E): The 3HB sextet resonance at 5.25 ppm overlaps with the methine PheLA resonance, so the methylene doublet resonances of 3.15 and 3.04 ppm and 2.58 and 2.48 ppm were used to show the presence of 3HB and PheLA respectively. The broad aromatic resonance at 7.21 ppm is also indicative of PheLA. (F): In addition to the 3HB sextet resonance at 5.25 ppm, a multiplet resonance at 5.12 ppm shows that the C2-methine of the MA repeat is present. The broad aromatic multiplet resonance at 7.28 ppm is also indicative of MA. (G): In addition to the 3HB sextet resonance at 5.25 ppm, two doublet resonances at 7.19 and 6.98 ppm show that the aromatic PA repeat is present, indicating incorporation of the phenylic unit into the polymer. (H): In addition to the 3HB sextet resonance at 5.25 ppm, two doublet resonances at 7.07 and 6.5 ppm show that the aromatic 5HM2FA repeat is present, indicating incorporation of the furanoic unit into the polymer.**

2.2 Impact of Genetic Engineering on PHA Production and Composition

The molecular weight of PHAs produced by the transgenic strain was compared to the bio-polyester produced by the wild-type of *C. necator* H16: gel-permeation chromatography (GPC) revealed that the M_W (or M_n) of the polymers derived from the engineered strain (not induced) was approx. 5-times lower than that produced by the wild-type (figure 3). Induction of the engineered strain (i.e., over-expression of the heterologous genes) resulted in another 5-fold reduction in molecular weight of the produced polymers while the polydispersity index (PDI) also increased. This trend was observed for all polymers that were analyzed by means of GPC (cf. table S2 & figure S22 – S35); hence, it appears that enzyme expression-level(s) and polymer chain-length are inversely correlated.

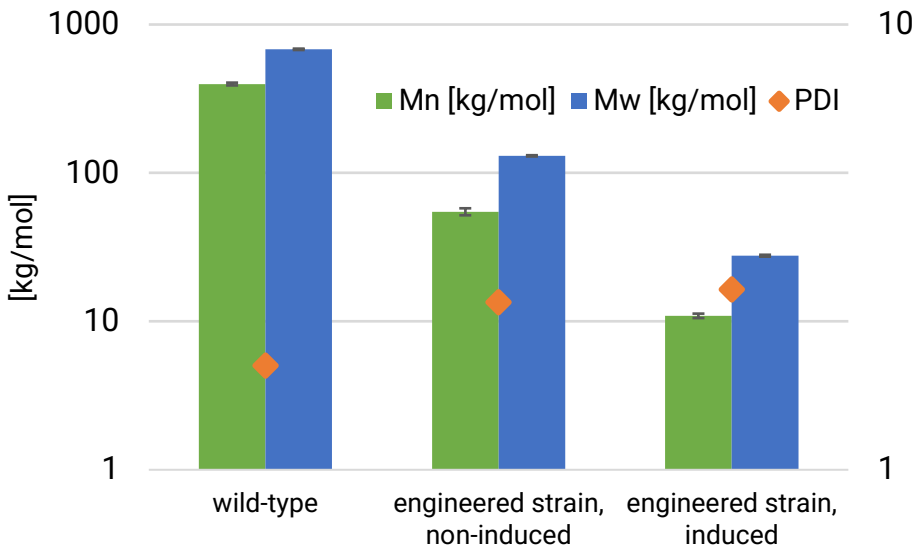

Figure 3: Comparison of molecular weight distribution (number average 'M_n' and weight average 'M_W') and polydispersity index (PDI) for PHA obtained from wild-type *C. necator* H16, and engineered *C. necator* H16 (Δ*phaC1* pCM66Tp$_{BAD}$:*hadA-phaC1437*, non-induced and fully induced, respectively). Molecular weights M_n and M_W are represented by green and blue bars, respectively, scaled on the left axis, while the PDI is represented by an orange diamond-shaped marker scaled on the right axis. The scales of both axes are logarithmic (base 10).

To determine the cause of this correlation, expression-levels of the PHA synthase (and CoA-transferase) during induced and non-induced conditions were compared qualitatively. In the latter case the proteins were not detected (cf. SI 1, figures S1 and S2), albeit catalytic activity of the PHA synthase evidently existed. The hypothesis is that the mutant PHA synthase 'PhaC1437' is highly active so that very little enzyme (from basal expression) is sufficient to catalyze the formation of PHAs. This would also explain the reduction in molecular weight of the polymer during induced conditions: the high activity of the enzyme in combination with high abundance of the catalyst could lead to (local) depletion of substrate and subsequently premature termination of chain-elongation. These observations are consistent with a congruent phenomenon, which was described when the gene order of the natural *phaCAB* operon was shuffled (36).

The molecular weight of the various aliphatic as well as aromatic PHAs from exogenously supplied precursors was on the same order of magnitude as for the non-supplemented PHA from the transgenic strains, as was the inverse correlation between enzyme expression and polymer molecular weight. The PDI of non-natural polyesters was generally higher than that of natural PHB (natural < 2 < non-natural) and highest when enzyme expression was fully induced. Extended data containing the M_W, M_n and PDI of the different PHAs can be found in table S2 of SI 1.

2.3 Thermal Properties of Non-Natural Bio-Polyesters

Polymers that contained a significant fraction of non-natural repeat-units were subject to differential scanning calorimetry (DSC), to determine the impact of the co-monomers on the thermal properties of the PHAs, as compared to the appropriate controls (i.e., polyester from wild-type and mutant strains not supplemented with non-natural precursors). Accounting for the results from GPC-analysis of the polymers, also the impact of heterologous enzyme expression on PHA characteristics was investigated. The compiled data is given in table 2, associated DSC plots can be found in SI 1 (figure S36 – S47).

Table 2: Melting points, glass-transition temperatures and molecular weights of a subset of the obtained PHAs (samples corresponding to the co-polymers described in table 1).

strain	induced	polymer	T_g [°C]	T_m [°C]	ΔH_c [J/g]	M_n [kg/mol]	PDI
H16 (*wild-type*)	#N/A	*P*3HB[a] #1	4	170	19	397.4	1.71
H16 Δ*phaC1 pct540 phaC1437*	no	*P*3HB	3	170	29	69.2	1.94
	yes	*P*3HB[b] #2	1	163	43	45.3	2.72
H16 Δ*phaC hadA phaC1437*	no	*P*3HB	4	169	42	54.8	2.38
	yes	*P*3HB[c] #3	1	164	34	10.9	2.54
H16 Δ*phaC1 pct540 phaC1437*	yes	*P*(3HB-*co*-4HB) ≈ 1:1	-24	160	27	25.2	2.94
H16 Δ*phaC hadA phaC1437*	yes	*P*(3HB-*co*-4HB-*co*-6HC) ≈ 100:5:2	-5	129	6	11.8	2.13
	yes	*P*(3HB-*co*-PheLA) ≈ 2:1	5	N/A	0	13.2	1.65
	yes	P(3HB-co-PA) ≈ 500:1	1	155	55	14.5	2.33
	yes	P(3HB-co-5HM2FA) ≈ 300:1	-1	159	53	13.7	3.28

3HB = 3-hydroxybutyrate, 4HB = 4-hydroxybutyrate, 6HC = 6-hydroxycaproate, PheLA = phenyllactate, PA = phloretate, 5HM2FA = 5-hydroxymethyl-2-furanoic acid, xHA = indeterminate hydroxycarbonate; T_g = glass-transition temperature, T_m = melting point, M_n = number average molecular weight, M_w = weight average molecular weight, PDI = polydispersity index (M_w/M_n); [a] natural PHB, [b,c] PHB with minor fraction of indeterminate hydroxycarbonate of natural origin (cf. figure S8 and S9).

The melting and glass transition temperatures (T_m and T_g, respectively) of the *P*3HB generated from both the *pct540*- and the *hadA*-strain are comparable to those of the wild-type *P*3HB (~170°C and ~4°C, respectively), whereas polymers generated under induction exhibit slightly lower T_m and T_g (~163°C and ~1°C, respectively). We attribute these slightly depressed melting points to the incorporation of small amounts of hydroxy acid comonomers of indeterminate structure upon high expression of the heterologous genes, as evidenced by minor resonances in the ^{1}H-NMR spectra (figures S8 and S9). The high melting point (~160°C) and relatively high heat of fusion (ΔH_c ~27 J/g, similar to *P*3HB), coupled with the low T_g (~-24°C, similar to *P*4HB) of the *P*(3HB-*co*-4HB) co-polymer derived from *C. necator* H16 Δ*phaC1* pCM66Tp$_{BAD}$:pct540-*phaC1437* provide strong evidence for a block co-polymer structure of the 3HB and 4HB repeat units (34). Further, the monomodal GPC trace (figure S27) observed for this sample are consistent with a block co-polymer structure. Moreover, minor resonances associated with 4HB-3HB and 3HB-4HB sequences in the NMR spectra (figure S11) are also consistent with a block-like organization of

the co-polymer, as reported previously (34). The relatively low T_m and T_g obtained for the *P*(3HB-*co*-4HB-*co*-6HC) co-polymer from *C. necator* H16 Δ*phaC1* pCM66Tp$_{BAD}$:*hadA-phaC1437* and the ^{1}H-NMR spectrum (figure S15) are consistent with a random organization of the repeat units. Similarly, the absence of a melting point for the *P*(3HB-*co*-PheLA) co-polymer formed by *C. necator* H16 Δ*phaC1* pCM66Tp$_{BAD}$:*hadA-phaC1437* (figure S43) and the NMR spectra (figure S17) are also consistent with a random co-polymer structure. These observations are consistent with the thermal properties and the resulting impacts on manufacturing applications, as previously discussed (14, 15, 24, 37). Also for the *P*(3HB-*co*-PA) and *P*(3HB-*co*-5HM2FA) co-polymers, the modest depression of the melting point (155 and 159°C vs. 170°C, respectively) is consistent with previous observations for the incorporation of small amounts of aromatic co-monomer units in aliphatic polyesters (38).

2.4 Production of Aromatic Polyesters under Autotrophic Conditions

C. necator can assimilate carbon dioxide, deriving the required reducing power in form of electrons from molecular hydrogen. Aerobic gas-fermentation, however, is costly and involves serious safety concerns (39, 40). Therefore, innovative solutions have been proposed that allow the *in-situ* formation of H_2 via electrochemical water splitting in a bio-electrochemical system (BES) (41-43). To demonstrate the sustainable production of novel aromatic polyesters via microbial electrosynthesis (MES), engineered *C. necator* H16 Δ*phaC1* pCM66Tp$_{BAD}$:*hadA-phaC1437* was cultivated in a single-chamber BES with CO_2 and electrical current as the only inputs (figure 4; also see SI 1, figure S48). In the membrane-less system, a constant current was applied, which led to water being split into oxygen at the anode and hydrogen at the cathode. CO_2 was continuously purged into the reactor, providing a gas-mix for chemolithotrophic growth of *C. necator*. The BES was inoculated from a pre-culture grown on a gaseous $H_2/CO_2/O_2$ mixture to facilitate adaptation to electroautotrophic conditions, which resulted in immediate growth in the BES with no lag-phase (figure 4). Preliminary experiments (data not shown) suggested that the amount of nitrogen-source to achieve limiting-conditions and initiate PHA accumulation was critical in the BES. Consequently, the concentration of ammonium salt in the medium was reduced and monitored throughout the experiment. Polymer precursor (PheLA) was added in two steps to control toxicity. Under conditions of MES, the growth rate was lower as compared to growth on gaseous $H_2/CO_2/O_2$ mixture (BES: $t_D \approx 26$ h vs. serum-bottles: $t_D \approx 10$ h, data not shown), which can be explained with mass-transfer limitations in the BES (ambient pressure and limited agitation). Nevertheless, significant biomass was accumulated, exceeding batch-experiments in serum-bottles: a maximum OD_{600} of 6.2, corresponding to a biomass concentration of ≈ 1.8 g/L, was reached after 90 h. The culture was harvested after 140 h and extraction of polyesters yielded an aromatic polyester, which was identified as *P*(3HB-*co*-PheLA) by means of ^{1}H-NMR spectroscopy (see SI 1, figure S18). The content of non-natural monomer was lower than on fructose (3HB:PheLA ratio of 50:3 under autotrophic vs. 2:1 under heterotrophic condition), which could be explained with lower concentration of precursor (1/4th i.e., 5 mM PheLA) and inducer (1/10th i.e., 0.1 g/L arabinose) in the microbial medium, as well as limited energy available to metabolism under autotrophic conditions (22). Nevertheless, this experiment demonstrates feasibility to produce aromatic PHAs from C1-feedstocks and electrical energy, which could electrify the materials industry and, when powered by renewable sources, would further close the loop to integrate this sector into a circular economy (3).

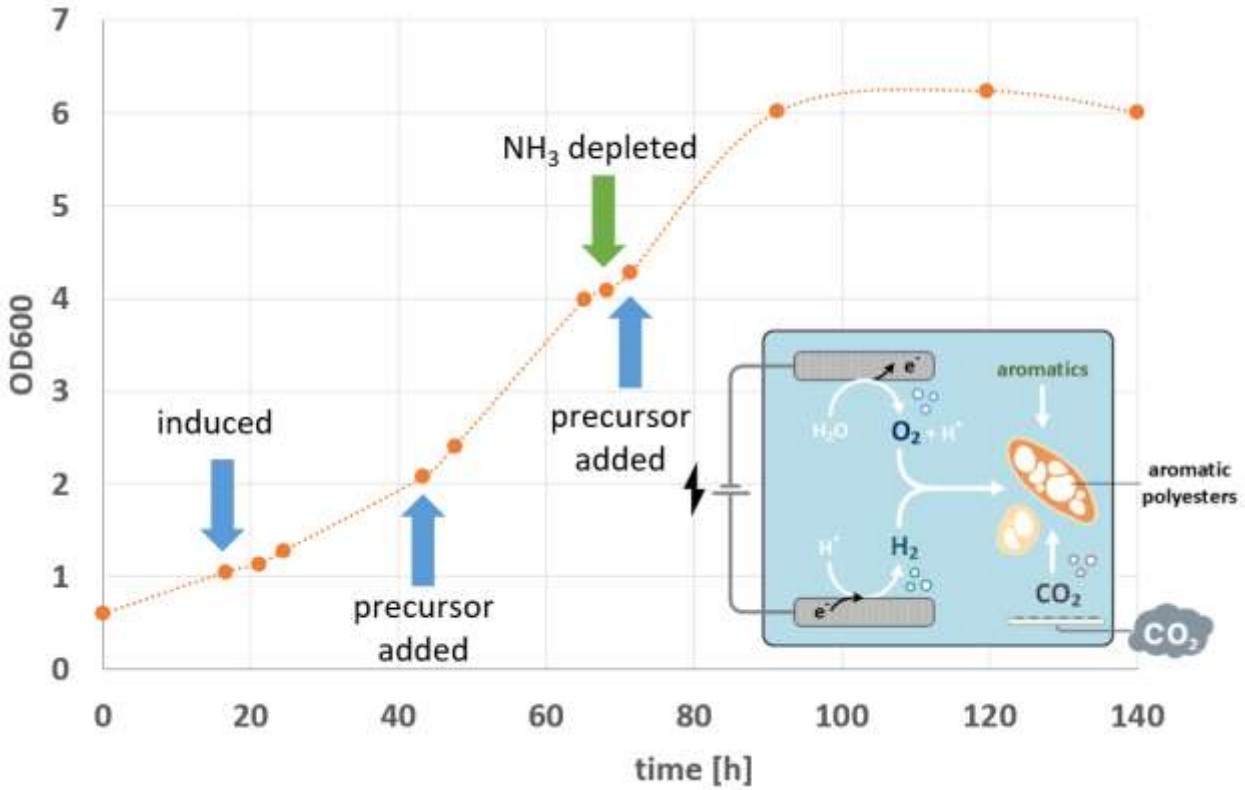

Figure 4: Cultivation-profile (growth measured as relative cell-density) of a representative experiment with transgenic *C. necator* H16 Δ*phaC1* pCM66Tp$_{BAD}$:*hadA-phaC1437* in a bio-electrochemical system (BES). Induction of expression of the heterologous genes, addition of aromatic polymer-precursor and depletion of nitrogen source were performed /determined as indicated. The insert on the bottom right shows a schematic of the BES, which evolves H_2 at the cathode and O_2 at the anode as electron-carrier and acceptor, respectively, for autotrophic growth and production of aromatic polyesters from CO_2 and electricity.

2.5 Metabolic Modelling of the Biosynthesis of Novel Bio-Polyesters

In support of the efforts described above, an *in-silico* analysis was conducted to assess feasibility of *de novo* production of the obtained co-polymers solely from basic carbon-sources. To limit the extent, only homo-polymers were considered. A reconstructed metabolic model of *C. necator* was amended with biochemical pathways for formation of several aliphatic or aromatic hydroxy acids and polymerization thereof, which in some cases were hypothetical. The full metabolic networks can be found in SI 3 (also see SI 1, figure S49). Using elementary flux-mode analysis (EMA), the production capacity for the different (non-natural) polyesters was compared on fructose, glycerol, acetate, formate and carbon dioxide + hydrogen, in terms of maximum theoretical product yield. The results are shown in figure 5, the corresponding numerical carbon-yields can be found in SI 3.

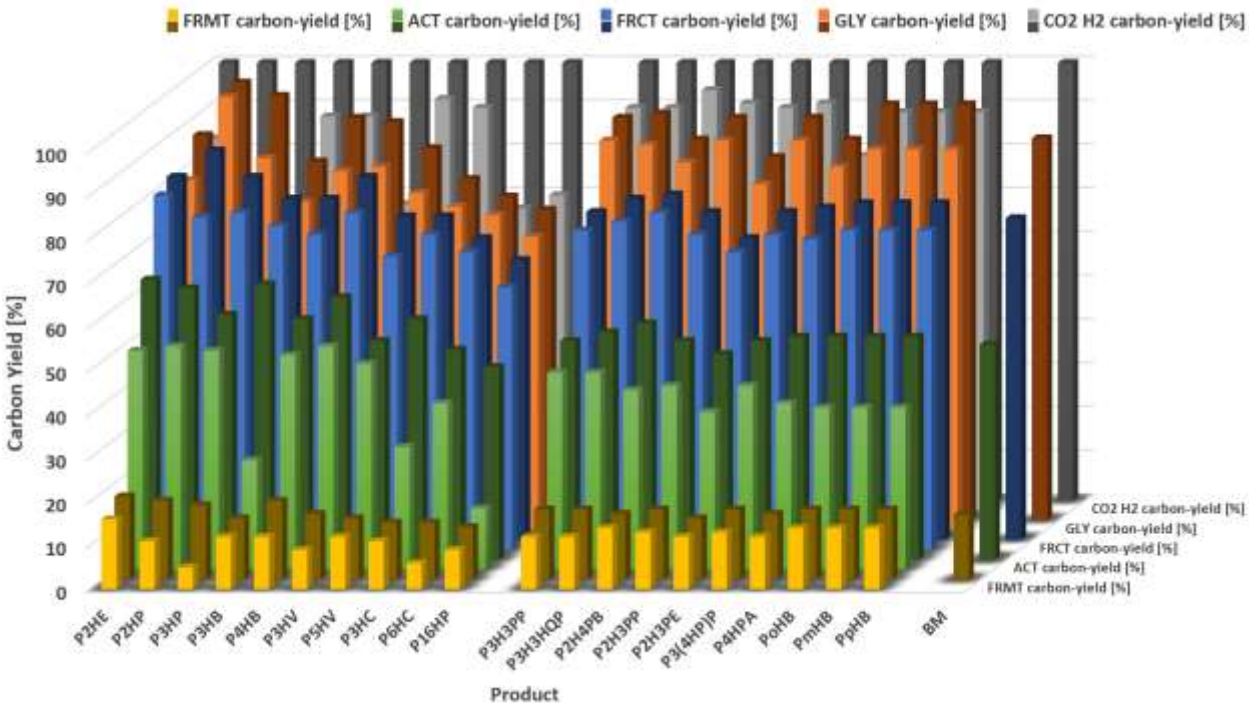

Figure 5: Theoretical maximum carbon-yields for a range of aliphatic as well as aromatic PHAs, producible from different carbon-/ energy-sources with engineered *C. necator*. Lighter shaded bars are product carbon-yields that allow for simultaneous growth, while darker shaded bars are absolute maximum theoretical product carbon-yields. The far-right columns represent the absolute maximum biomass yields, obtainable on the different carbon-sources. Substrates: FRMT = formate, ACT = acetate, FRC = fructose, GLY = glycerol; CO2 H2, carbon dioxide + hydrogen. Products: P2HE = poly(2-hydroxyethanoate), P2HP = poly(2-hydroxypropanoate) [poly(lactate)], P3HP = poly(3-hydroxypropanoate), P3HB = poly(3-hydroxybutyrate), P4HB = poly(4-hydroxybutyrate), P3HV = poly(3-hydroxyvalerate), P5HV = poly(5-hydroxyvalerate), P3HC = poly(3-hydroxycaproate), P6HC = poly(6-hydroxycaproate), P16HP = poly(16-hydroxypalmitate), P3H2PP = poly(3-hydroxy-3-phenylpropanoate), P3H2HQP = poly(3-hydroxy-3-hydroquinoyl-propanoate), P2H4PB = poly(2-hydroxy-4-phenylbutanoate), P2H3PP = poly(2-hydroxy-3-phenylpropanoate) [poly(phenyllactate)], P2H3PE = poly(2-hydroxy-3-phenylethanoate) [poly(mandelate)], P3(4HP)P = poly(3-(4-hydroxyphenyl)propanoate) [poly(phloretate)], P4HPA = 4-hydroxyphenylacetate, PoHB = poly(*orth*-hydroxybenzoate), PmHB = poly(*meta*-hydroxybenzoate), PpHB = poly(*para*-hydroxybenzoate), BM = biomass.

All pathways for formation of the considered aliphatic as well as aromatic PHAs appeared feasible within the employed network from all assessed feedstocks. Hence, the targeted non-natural bio-polyesters can theoretically be produced *de-novo*, without the need for supplement polymer-precursors, given that (A) metabolic engineering efforts to allow formation of the monomers are successful and (B) these are polymerizable. The latter will likely require discovery and/or engineering of novel PHA synthases, to expand and tailor the enzymes functionality.

Certain feedstocks appeared superior over others in terms of theoretical maximum yield: carbon-yields on formate were lowest, followed by acetate. Fructose and glycerol, as more reduced carbon-sources, could deliver higher yields, only surpassed by CO_2+H_2.[1] The near-100% carbon-efficiency on carboxy-hydrogen can be explained with the separation of carbon- and energy-source into two chemical species. This allows for flexibility in steady-state flux distributions, where, by means of the H_2 to CO_2 intake-ratio, as much energy as needed can be directed to recycling of CO_2. The real-world consequence of this finding is an imperative for process-control, to optimize the gas-mix and/or implement effective recycling of unused substrate. The low yields on formate are owed to the low energy that is chemically bound by this combined carbon- and energy-carrier. Much of the formate is simply converted to carbon dioxide to obtain reducing equivalents used to drive metabolism while little of the carbon is assimilated, analogous to expectations from a carboxy-hydrogen feed with fixed stoichiometry (low hydrogen to carbon dioxide ratio). Nevertheless, formate can be electrochemically regenerated from carbon dioxide (44). Therefore, if an economically viable and technically practical solution can be developed, a closed-loop recycling-system could effectively mimic a scenario where overall carbon-yields should approach those on carboxy-hydrogen, without the drawbacks of gas-transfer limitations (39).

[1] It should be noted that the *in-silico* model does not predict the phenotype that can be expected but is reflective of the leeway of the microbial system (i.e., cellular metabolism). *In-vivo*, many other factors can influence the actual idle state of the system. This includes kinetics, which are not respected in this particular type of metabolic model.

3 Conclusion

In this study we demonstrate the biosynthesis of various non-natural polyhydroxyalkanoates through co-polymerization of 3-hydroxybutyrate with bio-derivable aliphatic and aromatic hydroxy carbonic acids. Most significantly, we report the first ever bio-polyesters with aromatic rings in the backbone – the incorporation of a hydroxyphenylic and a hydroxyfuranoic acid into the polymer marks the introduction of the new class of "polyhydroxy*arylates*". These polymers are structurally analogous to polyethylene terephthalate (PET) and polyethylene furanoate (PEF) (18, 19), paving the way towards biological production of high-performance bioplastics. Further, also co-polymers containing arylaliphatic 2-hydroxy carbonates with the phenyl-group on a side chain of two, one and without residual carbons were obtained, properties of which can reportedly be comparable to polystyrene (PS) (17). With C3, C4 and C6 aliphatic ω-hydroxy acids also being polymerizable in the same system, also elastomers may be obtained (13, 14). Co-polymerization thereof with *para*-hydroxyphenylic or hydroxyfuranoic acids or even homopolymers of the newly polymerizable aromatics may ultimately yield biodegradable plastics with properties ranging from elastomers to resembling liquid crystal polymers like e.g. Vectran™ (19, 45).

The precursors for these bioplastics are available from waste and non-food carbon-sources (e.g., VFAs from anaerobic digestion, from lignin in case of phloretic acid (46, 47), or via 5-(hydroxymethyl)furfural (HMF) from lignocellulosic (48) as well as lignin-free biomass (49) in case of 5-hydroxymethyl-2-furanoic acid). Alternatively, hydroxy carbonic acids may be biosynthesized *in-situ* from single-carbon compounds such as carbon dioxide: using metabolic pathway modelling, the ability of *C. necator* to *de-novo* produce twenty PHAs was analyzed and found to be feasible, which highlights the potential for bio-production of advanced polyesters outgoing from sustainable carbon-sources. To substantiate this, we cultivated our transgenic strain in a bio-electrochemical system, proving that aromatic polyester can actually be formed under autotrophic conditions.

From the characterization of the obtained polymers, it appeared that expression-level of the PHA synthase and the molecular weight of the obtained polymer were inversely correlated. This finding has wide-ranging implications for strain engineering, as balancing the catalytic rate of the PHA synthase with substrate availability becomes critical to fine-tune polymer quality as well as composition. While extensive metabolic and process engineering will be required to realize the one-step bioproduction of these polymers, recent developments in synthetic biology and advancement of genetic tools for *C. necator* have brought this strategy for valorization of CO_2 within reach (4, 22). Overall, the biosynthesis of novel aromatic polyesters as demonstrated in this work is an important step towards leveraging biomanufacturing for carbon-neutral and potentially even carbon-negative production of bio-replacement materials (5). Truly renewable bioplastics with a wide range of properties may eventually enable creation of a sustainable chemical manufacturing industry and circular economy.

4 Materials and Methods

4.1 Strains and Media

Rich Broth (RB) was composed of Nutrient Broth (16 g/L), Yeast Extract (10 g/L) and ammonium sulfate (5 g/L). When applicable, kanamycin (kan, 300 mg/L for *C. necator* and 100 mg/L for *E. coli*) and/or diaminopimelate (DAP, 300 µM / 100 mg/L) were added.

Modified Mineral Salts Medium (MSM) was composed as described before (50); in brief, it contained 6.4 g/L Na_2HPO_4, 4.8 g/L KH_2PO_4, 1 g/L NH_4Cl, $MgSO_4$ 0.36 g/L, $CaCl_2 \times 2H_2O$ 0.088 g/L and 1 mL/L of 1000× trace elements (0.2 g/L $CoCl_2 \times 6H_2O$, 0.01 g/L $CuSO_4 \times 5H_2O$, 0.15 g/L $FeSO_4 \times 7H2O$, 0.06 g/L NH4Fe(III) citrate, 0.3 g/L H_3BO_4, 0.035 g/L $MnCl_2 \times 4H_2O$, 0.035 g/L $(NH_4)6Mo_7O_{24} \times 4H_2O$, 0.031 g/L $NiSO_4 \times 7H_2O$, 0.1 g/L $ZnSO_4 \times 7H_2O$). The medium was supplemented with 20 g/L fructose as carbon- and energy-source and 300 mg/L kanamycin (to ensure plasmid maintenance) when applicable.

For (electro)autotrophic cultivations modified minimal medium that contained no chlorine salts (to avoid electrocatalytic formation of Cl_2) was adapted from literature (51). Specifically, the "electro-medium" contained 4.52 g/L Na_2HPO_4, 5.17 g/L $NaH_2PO_4 \times 2H_2O$, 0.17 g/L K_2SO_4, 0.097 g/L $CaSO_4 \times 2H_2O$, 0.8 g/L $MgSO_4 \times 7H_2O$, 0.94 g/L $(NH_4)_2SO_4$ and 350 µL/L of 2857× trace elements (10 g/L $FeSO_4 \times 7H_2O$, 2.4 g/L $MnSO_4 \times H_2O$, 2.4 g/L $ZnSO_4 \times 7H_2O$, 0.48 g/L $CuSO_4 \times 5H_2O$, 1.8 g/L $Na_2MoO_4 \times 2H_2O$, 1.5 g/L $NiSO_4 \times 6H_2O$, 0.04 g/L $Co(NO_3)_2 \times H_2O$ in 0.1 M HCl). The medium was supplemented with 100 mg/L kanamycin to ensure plasmid maintenance. For production of PHA in the bio-electrochemical system (BES), the initial concentration of $(NH_4)_2SO_4$ was further reduced to 5 mM to achieve nitrogen-limiting conditions.

E. coli WM3064 (a B2155 derivative), an auxotrophic RP4 mobilizing λ*pir* cell-line (52), was a gift from the Spormann Laboratory (Stanford University). WM3064 was routinely cultivated on LB (solid or liquid, at 30°C) supplemented with DAP (300 µM) and kanamycin (50 µg/mL) as applicable. *C. necator* H16 and *C. necator* H16 Δ*phaC1* were gifts from the Silver Laboratory (Harvard Medical School) (23) and routinely grown at 30°C on solid or liquid RB or MSM. A comprehensive list of the strains used and constructed in this study can be found in table 3.

Table 3: Strains used in this study.

Strain	Genotype	Source
E. coli WM3064	thrB1004 pro thi rpsL hsdS lacZΔM15 RP4-1360 Δ(araBAD)567 ΔdapA1341::[erm pir]	(52)
E. coli WM3064 pCM66Tp$_{BAD}$:RFP	WM3064 kan^R drFP583	this study
E. coli WM3064 pCM66Tp$_{BAD}$:*pct540-phaC1437*	WM3064 kan^R pct540 phaC1437	this study
E. coli WM3064 pCM66Tp$_{BAD}$:*hadA-phaC1437*	WM3064 kan^R hadA phaC1437	this study
C. necator H16		(23)
C. necator H16 Δ*phaC1*	H16 ΔphaC1	(23)
C. necator H16 Δ*phaC1* pCM66Tp$_{BAD}$:RFP	H16 ΔphaC1 drFP583	this study
C. necator H16 Δ*phaC1* pCM66Tp$_{BAD}$:*pct540-phaC1437*	H16 ΔphaC1 pct540 phaC1437	this study
C. necator H16 Δ*phaC1* pCM66Tp$_{BAD}$:*hadA-phaC1437*	H16 ΔphaC1 hadA phaC1437	this study

4.2 Genetic Engineering

4.2.1 Vector Construction

The RK2/RP4 oriV (IncP) plasmid pCM66T was obtained from AddGene. pBBR1MCSp$_{BAD}$:RFP, a derivate of pBBR1MCS with a red fluorescent protein (drFP583) under control of the araBAD promoter, was a gift from the Silver Laboratory (Harvard Medical School). pCM66Tp$_{BAD}$:RFP was constructed by cloning the P$_{BAD}$-RFP cassette into pCM66T using NEBuilder, replacing the polylinker and its regulatory elements. The protein sequences of Q9L3F7_CLOPR (*pct*), Q188I3_PEPD6 (*hadA*) and B9W0T0_9PSED (*phaC*) were derived from UniProt, implementing the previously described mutations (V193A for *pct540* and E130D, S325T, S477G, Q481K for *phaC1437*) as applicable. The sequences were fused with a C-terminal tripleglycine-spacer and tetracysteine- (Lumio)-tag and codon-optimized for expression in *C. necator* with GeneArt® (Invitrogen). The genes were arranged in a single operon under control of the araBAD promoter in combination with the strong T7 ribosomal binding-site and a T7Te – rrnB T1 double-terminator. The plasmids pCM66Tp$_{BAD}$:*pct540-phaC1437* and pCM66Tp$_{BAD}$:*hadA-phaC1437* were constructed by GenScript Biotech, cloning the synthetic operons containing *pct540* & *phaC1437* and *hadA* & *phaC1437*, respectively, into pCM66Tp$_{BAD}$:RFP, replacing the RFP (see SI 2 for plasmid maps).

4.2.2 Conjugation

Plasmid vectors were introduced into *C. necator* by bacterial conjugation, using the *E. coli* donor-strain WM3064, which had been transformed with the plasmid vectors pCM66Tp$_{BAD}$:*pct540-phaC1437* and pCM66Tp$_{BAD}$:*hadA-phaC1437* using the Mix & Go! *E. coli* Transformation Kit (Zymo).

Conjugation was performed as follows: the recipient strain (*C. necator* H16 Δ*phaC1*) was incubated at 30°C on RB plates over night; simultaneously the donor strains (WM3064) carrying the plasmid vectors were

incubate at 30°C on LB plates with kan and DAP. From the agar-plates, liquid cultures of the donor strains were inoculated (LB with kan and DAP) and incubated overnight with shaking at 30°C. Likewise RB was inoculated with the recipient strain and incubated overnight with shaking at 30°C. On the next day 3 mL of LB with DAP (but no antibiotics) per donor-strain were each inoculated with 6 µL of overnight culture and incubated with shaking at 37°C. Similarly, a matching number of recipient strain cultures were inoculated combining 20 µL of overnight culture and 10 mL of RB each, which were incubated with shaking at 30°C. After 4 h the cultures were combined using 3 mL of the *E. coli* and 10 mL of the *C. necator* culture. Cells were collected by centrifugation (4816×g for 10 min) and the supernatant was discarded. The cell-pellet was re-suspended in 200 µL of RB with DAP and a "blob" of each cell mixture was pipetted on an RB plate with DAP. The agar-plates were incubated at 30°C overnight with the place facing up. On the next day, a single scoop of biomass was collected with an inoculation loop and suspended into 500 µL of 25% glycerol. The suspension was diluted 1:10 and 1:100 and all three concentrations were plated on separate RB plates with kan. The plates were incubated at 30°C; colonies that appeared after about two days were picked and isolated on separate RB plates with kan for propagation and screening.

4.3 Cultivation of Microbes

4.3.1 Cultivation of *C. necator* in Shake- and Serum-Flasks

Liquid cultures under heterotrophic conditions were maintained in 500 mL vented, baffled shake-flasks (WHEATON® Erlenmeyer Flasks with DuoCap®, DWK Life Sciences), incubated at 30°C with shaking at 180 rpm on an innova 2300 platform shaker (New Brunswick Scientific). For feeding experiments, precultures of the engineered *C. necator* strains were inoculated in liquid RB + kan (50 mL) from solid RB + kan and grown over-night. In the morning the medium was exchanged for MSM + kan, washing and diluting the culture 1:2 (in 100 mL). In the afternoon the seed-culture was washed again with MSM and again diluted 1:2 (in 200 mL) with MSM + kan + polymer-precursor. In the evening the culture was induced with 1 g/L arabinose unless indicated otherwise. Growth was monitored by means of OD (absorbance at 600 nm), accompanied by collection of supernatant samples, as applicable. The cultures were harvested after approx. 48 h or when no further increase in biomass density was observed.

Precultures for the bio-electrochemical system were done in two steps: 125 mL serum bottles (25 mL liquid medium, 100 mL gas headspace) were filled with 25 mL “electro-medium” and sealing with butyl rubber stoppers secured with crimp-caps. Initially starting the cultures on 1 g/L fructose, the medium was inoculated with the engineered *C. necator* from solid RB + kan and incubated at 30°C with shaking at 200 rpm overnight. Subsequently, these cultures were transferred to autotrophic conditions on $H_2/CO_2/O_2$: the initial gas-phase was H_2/CO_2 (80%/20%) at 17 psi, which was further pressurized to 22 psi with O_2 (100%), resulting in a final gas composition of 64:16:20 ($H_2/CO_2/O_2$). After three days of incubation, autotrophic growth was observed, reaching a maximum cell density of OD 3.8±0.15 within 48 h (data not shown). For transfer to the BES, exponentially growing cultures were harvested at an OD of ≈ 0.7 (by centrifugation at 4000×g for 6 min) and re-suspended in 25 mL of fresh medium.

4.3.2 Cultivation of *C. necator* in the Bio-Electrochemical System

The bio-electrochemical system was a custom (500 mL) glass vessel with rubber-stopper side ports (Adams & Chittenden Scientific). The reactor was operated membrane-less as three-electrode setup, magnetically stirred at 300 rpm. The cathode was a Nickel-Molybdenum alloy on graphite support (total surface area 50 cm^2), which has been characterized previously and found to evolve H_2 at 100% selectivity under biologically relevant conditions (53, 54). The anode was platinized titanium mesh (PLANODE1X4, TWL) and an Ag/AgCl reference electrode (NaCl saturated; RE-5B, BASi®), both of which were inserted via a rubber stopper side-port. The electrochemical reactor was controlled by applying a constant current of 100 mA using a multichannel potentiostat (VMP3; BioLogic Science Instruments, EC-Lab 11.21), providing a constant electron flow and therefore constant rate of H_2 and O_2. In abiotic pre-tests (data not shown) the reactor headspace was analyzed (via GC) to confirm that H_2 and O_2 were the sole gaseous products.
The reactor was filled with 300 mL medium, and CO_2 was supplied via a mass flow controller (EL-Flow F-100D, Bronkhorst®) at a constant flowrate of 1 mL/min. Before inoculation, the BES was operated for at least one hour under abiotic conditions to saturate the medium with the gases. The reactor was inoculated with 25 mL of concentrated cell-suspension from exponentially growing, autotrophic cultures, to achieve a starting OD between 0.5 and 0.6 (and final liquid volume of 325 mL). Preliminary tests showed that under autotrophic growth conditions accumulation of PHA required tight limitation of the nitrogen-source. Therefore, the initial concentration of ammonium salt in the BES was reduced to 5 mM and consumption was monitored (using "EasyStrips" Ammonia Test Strips, Tetra® GmbH with a sensitivity < 0.5 mg/L) throughout the experiment. Growth and pH were also measured by drawing samples manually. After 24 h of stable growth the culture was induced with arabinose (0.1 g/L final conc.). Approx. 24 h after induction, the first dose of precursor was added (2.5 mM final conc.), and the second dose (additional 2.5 mM to reach a total of 5 mM) when the nitrogen-source was depleted. The experiment was terminated when no further growth was observed. Cells were harvested via centrifugation followed by polymer extraction. Pictures of the set up can be found in SI 1 (figure S33).

4.4 Extraction of PHAs

Liquid cultures of *C. necator* were harvested by centrifugation and the cell pellet was freeze dried. After determining the dry cell weight (CDW), PHAs were extracted by lysis of the cell pellet (wet or dry) with 10% sodium hypochlorite solution (Honeywell Fluka™) using approx. 0.2 L/g_{CDW}. The pellet was completely suspended and incubated at room-temperature for 20 min with intermittent mixing. The suspension was diluted with water 1:2 and centrifuged at 4816×g for 20 min. As only remaining solids, the PHAs were washed twice with water and once with methanol, repeating the centrifugation step. The dried polymer was weight to determine the product yield, dissolved in chloroform, filtered through a 0.2 µm PTFE "Titan3™" (Thermo Scientific™) syringe filter and dried for analysis.

4.5 Protein Extraction and Detection

Culture derived from distinct time-points of a batch cultivation (exponential-phase / stationary-phase) was collected (sample volume [mL] ≈ 10 / OD_{600}) and cells were pellet by centrifugation (4816×g at 4°C for 10 min). The pellet was washed with purified water and stored as cell-paste at -20°C for later processing.

For extraction of proteins, CelLytic™ B (Sigma) was used as per manufacturer's directions (approx. 1 mL per cells from 10 mL culture at an OD of 1), in combination with Protease Inhibitor Cocktail (Sigma-Aldrich). The mixture was vortexed for 2 min to lyse the cells and extract the soluble protein. Centrifugation (4816×g for 10 min) pelleted the cell debris; the supernatant, which contained the soluble proteins, was separated. Total protein concentration was determined using the BCA Protein Assay Kit (Pierce™). Using the Lumio™ Green Detection Kit (ThermoFisher) as per manufacturer's directions, 10 µg crude protein extract of each sample were prepared for gel electrophoresis. Size-separation was performed on a Bolt™ 4-12% Bis-Tris Plus Gel (ThermoFisher), run at 150 V for approx. 40 min with Bolt™ MES SDS Running Buffer (ThermoFisher). The marker was BenchMark™ Fluorescent Protein Standard (ThermoFisher). A Gel-Doc (BioRad) was used to visualize fluorescent-conjugated proteins. For visualization of all proteins, the gels were re-stained with One-Step Lumitein™ Protein Gel Stain (Biotium) as per manufacturer's directions and imaged again as before.

4.6 Analytics

4.6.1 Determination of OD and Cell Dry-Weight Correlation

Microbial growth was characterized by measuring the optical density at 600 nm (OD_{600}) with a DR2800™ Portable Spectrophotometer (HACH) for shake-flask cultures and Ultrospec™ 2100 pro (Amersham BioSciences) in case of MES using the BES.

A correlation between OD_{600} and biomass (BM) concentration was determined gravimetrically (data not shown) from batch shake-flask cultivations with the wild-type (five samples) and engineered strains (15 samples) of *C. necator*. Shake-flask cultures of 50 mL with different cell densities were harvested via centrifugation and vacuum dried. The quotient of OD_{600}/BM (dry weight in mg) averaged from all samples was 0.3±0.04, such that the correlation is: $OD_{600} \times 0.3$ = BM [g/L].

4.6.2 HPLC

Quantification of fructose in the culture-broth was based on a previously published HPLC-method for detection of organic acids (55). In short, the procedure was as follows: Samples (1 mL) were filtered (PVDF or PES syringe filters, 0.2 µm pore-size) and diluted 1:100 into HPLC sampling vials. Analysis of 50 µL sample-volume was performed on an 1260 Infinity HPLC system (Agilent), using an Aminex HPX87H column (BioRad) with 5 mM H_2SO_4 as the eluent, at a flow rate of 0.7 mL/min. Fructose was identified and quantified by comparison to standards (3 g/L, 1.5 g/L, 0.6 g/L, 0.3 g/L, 0.15 g/L, 0.03 g/L), according to retention time (8.8 min) using a refractive index detector (35°C).

4.6.3 Nuclear Magnetic Resonance (NMR) Spectroscopy

NMR samples were prepared as previously reported (56). In short, a few mg of polymer were dissolved in deuterated chloroform and ^{1}H-NMR as well as ^{13}C-NMR spectra were recorded at 25°C on a Unity INOVA™ 500 NMR Spectrometer (Varian Medical Systems) with chemical shifts referenced in ppm relative to tetramethylsilane.

4.6.4 Gas Chromatography–Mass Spectrometry (GC-MS)

GC-MS analysis was adopted from literature (23). In brief, between 3 and 70 mg of extracted polymer was transferred to crimped vials, to which 2 mL chloroform and 2 mL methanol with 15% HCl were added. The vials were closed and incubated for one to two hours at 100°C. Vials were cooled on ice and the content was combined with 4 mL H_2O in a screw-cap glass vial. The mixture was homogenized, and phases were separated by centrifugation at 4816×g for 10 min. The chloroform phase (bottom) was transferred into a GC-MS vial for analysis. Samples were analyzed on a 7890 / 5975 inert XL GCMS (Agilent Technologies) with a J&W CP-TAP CB column CP7483 (Agilent Technologies). Analytes were heated on a gradient from 35°C to 250°C at 2°C/min. Co-polymers were detected with mass spectra of hydroxy acid methyl esters at m/z = 1 – 3 and NIST Mass Spectral Library.

4.6.5 Gel Permeation Chromatography (GPC)

Gel Permeation Chromatography (GPC) TSKgel SuperHZM-H column (Tosoh) connected in series with a DAWN multiangle laser-light scattering (MALLS) detector and an Optilab T-rEX differential refractometer (Wyatt Technology). Polystyrene calibrated (from M_p = 500 – 275,000 g/mol) molecular weights were determined using a GPCmax autosampler at 25°C at a flow rate of 1 mL/min.

4.6.6 Differential Scanning Calorimetry (DSC)

Differential Scanning Calorimetry (DSC) was conducted on a Q2500 (TA Instruments) using a heating and cooling rate of 10 °C/min and a nitrogen flow rate of 50 mL/min. Heat flow (mW) was recorded relative to an empty reference pan. Glass transition temperatures and melting points were determined on the second heating scan at a heating rate of 10°C/min. The crystallization enthalpy was determined from the area of the crystallization peak of the cooling curve (Eq. 1).

$$\text{heat of crystallisation} = \frac{\text{area under crystalisation peak}}{\text{cooling rate}} \Leftrightarrow \Delta H_c = \frac{\mathrm{W{\times}°C/g}}{\mathrm{°C/s}} = \frac{\mathrm{W \times s}}{\mathrm{g}} = \frac{\mathrm{J}}{\mathrm{g}} \qquad \text{Eq. 1}$$

4.7 Metabolic Modelling

Based on previously established metabolic networks of *C. necator* for elementary flux-mode analysis (57, 58), refined and fully compartmentalized model was fundamentally re-constructed. Expansions were made to describe C1- and energy-metabolism more precisely (28, 59) and the model was amended with additional carbon assimilation and product formation pathways (see SI 1, figure S49), deducted from metabolic databases such as KEGG (60, 61). Reaction thermodynamics of the heterologous pathways were verified using the eQuilibrator for estimation of the Gibbs free energy $\Delta_r G'^m$ (62).

Elementary flux modes were calculated in MATLAB® (MathWorks®), using 'FluxModeCalculator' (63), and evaluated as described previously (64). Balances were established around boundary reactions, allowing carbon-yields [C-mol/C-mol] for all products to be determined.

Supporting Information

- Appendix: Documentation containing growth-data, visualization of protein gels and correlation of both, additional NMR and GC-MS spectra, as well as GPC and DSC plots and resulting data (SI 1)

- Datasets: Annotated vector maps of genetic constructs (SI 2) and spreadsheet containing metabolic models of *C. necator* (SI 3) including pathways to formation of PHAs

Acknowledgements

This study was supported by a Stanford Natural Gas Initiative (NGI) program grant (SPO #139138), as well as NASA grant or cooperative agreement award number NNX17AJ31G. Any opinions, findings, and conclusions or recommendations expressed in this material are those of the author and do not necessarily reflect the views of the National Aeronautics and Space Administration (NASA). Part of this work was performed at the Stanford Nano Shared Facilities (SNSF), supported by the National Science Foundation (NSF) under award ECCS-2026822.

Author Contributions

NJHA conceived the study, designed, and conducted the experiments and composed the manuscript. VEP, FK, MZ performed analytics (NMR & GPC & DSC, HPLC, GC-MS, respectively), SNN helped with strain construction. FK designed and conducted experiments in the bio-electrochemical system. RWW and CSC supported and advised the project. All authors have read and approved the final manuscript.

Competing Interests

MZ and SNN are employees of Circe Bioscience Inc., a biomanufacturing company with financial interest in the microbiological production of foods from single-carbon feedstocks using lithoautotrophic bacteria. All other authors declare no competing interests.

References

1. J. Smith, S. Vignieri, A devil's bargain. *Science* **373**, 34-35 (2021).
2. R. Geyer, J. R. Jambeck, K. L. Law, Production, use, and fate of all plastics ever made. *Science Advances* **3**, e1700782 (2017).
3. S. R. Nicholson, N. A. Rorrer, A. C. Carpenter, G. T. Beckham, Manufacturing energy and greenhouse gas emissions associated with plastics consumption. *Joule* **5**, 673-686 (2021).
4. S. Y. Lee *et al.*, A comprehensive metabolic map for production of bio-based chemicals. *Natue Catalysis* **2**, 18-33 (2019).
5. P. Stegmann, V. Daioglou, M. Londo, D. P. van Vuuren, M. Junginger, Plastic futures and their CO2 emissions. *Nature* **612**, 272-276 (2022).
6. X. Chen, N. Yan, A brief overview of renewable plastics. *Materials Today Sustainability* **7-8**, 100031 (2020).
7. L. D. Ellis *et al.*, Chemical and biological catalysis for plastics recycling and upcycling. *Nature Catalysis* **4**, 539-556 (2021).
8. G. Atiwesh, A. Mikhael, C. C. Parrish, J. Banoub, T.-A. T. Le, Environmental impact of bioplastic use: A review. *Heliyon* **7**, e07918 (2021).
9. J. M. Clomburg, A. M. Crumbley, R. Gonzalez, Industrial biomanufacturing: The future of chemical production. *Science* **355**, aag0804 (2017).
10. A. M. Brandon, C. S. Criddle, Can biotechnology turn the tide on plastics? *Curr Opin Biotech* **57**, 160-166 (2019).
11. P. J. Strong *et al.*, The Opportunity for High-Performance Biomaterials from Methane. *Microorganisms* **4**, 11 (2016).
12. Z. Li, J. Yang, X. J. Loh, Polyhydroxyalkanoates: opening doors for a sustainable future. *NPG Asia Materials* **8**, e265-e265 (2016).
13. B. Andreeßen, N. Taylor, A. Steinbüchel, V. Müller, Poly(3-Hydroxypropionate): a Promising Alternative to Fossil Fuel-Based Materials. *Applied and Environmental Microbiology* **80**, 6574-6582 (2014).
14. C. Utsunomia, Q. Ren, M. Zinn, Poly(4-Hydroxybutyrate): Current State and Perspectives. *Frontiers in Bioengineering and Biotechnology* **8** (2020).
15. A. G. Aduhene *et al.*, Poly(3-hydroxypropionate): Biosynthesis Pathways and Malonyl-CoA Biosensor Material Properties. *Frontiers in Bioengineering and Biotechnology* **9** (2021).
16. M. Ishii-Hyakutake, S. Mizuno, T. Tsuge, Biosynthesis and Characteristics of Aromatic Polyhydroxyalkanoates. *Polymers* **10**, 1267 (2018).
17. T. Liu *et al.*, Synthesis of Polymandelide: A Degradable Polylactide Derivative with Polystyrene-like Properties. *Macromolecules* **40**, 6040-6047 (2007).
18. T. L. Simmons, G. L. Baker, Poly(phenyllactide): Synthesis, Characterization, and Hydrolytic Degradation. *Biomacromolecules* **2**, 658-663 (2001).
19. X. Jin, C. Carfagna, L. Nicolais, R. Lanzetta, Synthesis and characterization of potentially biodegradable thermotropic polyesters based on *p*-hydroxybenzoic acid and glycolic acid. *Journal of Polymer Science Part A: Polymer Chemistry* **32**, 3115-3122 (1994).
20. A. Reina, A. Gerken, U. Zemann, H. R. Kricheldorf, New polymer syntheses, 101. Liquid-crystalline hyperbranched and potentially biodegradable polyesters based on phloretic acid and gallic acid. *Macromolecular Chemistry and Physics* **200**, 1784-1791 (1999).
21. S. J. Park *et al.*, Metabolic engineering of *Ralstonia eutropha* for the production of polyhydroxyalkanoates from sucrose. *Biotechnology and Bioengineering* **112**, 638-643 (2015).
22. J. Panich, B. Fong, S. W. Singer, Metabolic Engineering of *Cupriavidus necator* H16 for Sustainable Biofuels from CO2. *Trends in Biotechnology* **39**, 412-424 (2021).
23. S. N. Nangle *et al.*, Valorization of CO2 through lithoautotrophic production of sustainable chemicals in *Cupriavidus necator*. *Metabolic Engineering* **62**, 207-220 (2020).
24. S. Mizuno, A. Hiroe, T. Fukui, H. Abe, T. Tsuge, Fractionation and thermal characteristics of biosynthesized polyhydoxyalkanoates bearing aromatic groups as side chains. *Polymer Journal* **49**, 557-565 (2017).
25. J. E. Yang *et al.*, One-step fermentative production of aromatic polyesters from glucose by metabolically engineered *Escherichia coli* strains. *Nat Commun* **9**, 79 (2018).

26. T. H. Yang *et al.*, Biosynthesis of polylactic acid and its copolymers using evolved propionate CoA transferase and PHA synthase. *Biotechnology and Bioengineering* **105**, 150-160 (2010).
27. J.-G. Rosenboom, D. K. Hohl, P. Fleckenstein, G. Storti, M. Morbidelli, Bottle-grade polyethylene furanoate from ring-opening polymerisation of cyclic oligomers. *Nature Communications* **9**, 2701 (2018).
28. N. J. Claassens *et al.*, Phosphoglycolate salvage in a chemolithoautotroph using the Calvin cycle. *Proceedings of the National Academy of Sciences* **117**, 22452-22461 (2020).
29. T. Tsuge, K. Tanaka, M. Shimoda, A. Ishizaki, Optimization of l-lactic acid feeding for the production of poly-d-3-hydroxybutyric acid by *Alcaligenes eutrophus* in fed-batch culture. *Journal of Bioscience and Bioengineering* **88**, 404-409 (1999).
30. S. L. Riedel, J. Lu, U. Stahl, C. J. Brigham, Lipid and fatty acid metabolism in *Ralstonia eutropha*: relevance for the biotechnological production of value-added products. *Applied Microbiology and Biotechnology* **98**, 1469-1483 (2014).
31. C. Arenas-López *et al.*, The genetic basis of 3-hydroxypropanoate metabolism in *Cupriavidus necator* H16. *Biotechnology for Biofuels* **12**, 150 (2019).
32. T. Fukui, M. Suzuki, T. Tsuge, S. Nakamura, Microbial Synthesis of Poly((R)-3-hydroxybutyrate-co-3-hydroxypropionate) from Unrelated Carbon Sources by Engineered *Cupriavidus necator*. *Biomacromolecules* **10**, 700-706 (2009).
33. N. Lindenkamp, M. Schürmann, A. Steinbüchel, A propionate CoA-transferase of *Ralstonia eutropha* H16 with broad substrate specificity catalyzing the CoA thioester formation of various carboxylic acids. *Applied Microbiology and Biotechnology* **97**, 7699-7709 (2013).
34. D. Hu *et al.*, Biosynthesis and Characterization of Polyhydroxyalkanoate Block Copolymer P3HB-*b*-P4HB. *Biomacromolecules* **12**, 3166-3173 (2011).
35. J. C. A. Flanagan, J. Myung, C. S. Criddle, R. M. Waymouth, Poly(hydroxyalkanoate)s from Waste Biomass: A Combined Chemical–Biological Approach. *ChemistrySelect* **1**, 2327-2331 (2016).
36. A. Hiroe, K. Tsuge, C. T. Nomura, M. Itaya, T. Tsuge, Rearrangement of gene order in the phaCAB operon leads to effective production of ultrahigh-molecular-weight poly[(R)-3-hydroxybutyrate] in genetically engineered *Escherichia coli*. *Appl Environ Microbiol* **78**, 3177-3184 (2012).
37. S. Mizuno, S. Katsumata, A. Hiroe, T. Tsuge, Biosynthesis and thermal characterization of polyhydroxyalkanoates bearing phenyl and phenylalkyl side groups. *Polymer Degradation and Stability* **109**, 379-384 (2014).
38. U. Witt, R.-J. Müller, W.-D. Deckwer, New biodegradable polyester-copolymers from commodity chemicals with favorable use properties. *Journal of environmental polymer degradation* **3**, 215-223 (1995).
39. C. H. Calvey *et al.*, Improving growth of *Cupriavidus necator* H16 on formate using adaptive laboratory evolution-informed engineering. *Metabolic Engineering* **75**, 78-90 (2023).
40. M. Pavan *et al.*, Advances in systems metabolic engineering of autotrophic carbon oxide-fixing biocatalysts towards a circular economy. *Metabolic Engineering* **71**, 117-141 (2022).
41. K. K. Sakimoto *et al.*, Physical Biology of the Materials–Microorganism Interface. *Journal of the American Chemical Society* **140**, 1978-1985 (2018).
42. T. Krieg, A. Sydow, S. Faust, I. Huth, D. Holtmann, CO2 to Terpenes: Autotrophic and Electroautotrophic α-Humulene Production with *Cupriavidus necator*. *Angewandte Chemie International Edition* **57**, 1879-1882 (2018).
43. C. Liu, B. C. Colón, M. Ziesack, P. A. Silver, D. G. Nocera, Water splitting–biosynthetic system with CO2 reduction efficiencies exceeding photosynthesis. *Science* **352**, 1210-1213 (2016).
44. M. F. Philips, G.-J. M. Gruter, M. T. M. Koper, K. J. P. Schouten, Optimizing the Electrochemical Reduction of CO2 to Formate: A State-of-the-Art Analysis. *ACS Sustainable Chemistry & Engineering* **8**, 15430-15444 (2020).
45. S. Cai *et al.*, Synthesis and Properties of Bio-based Copolyesters Based on Phydroxyphenylpropionic Acid. *Journal of Polymers and the Environment* 10.1007/s10924-022-02732-7 (2022).
46. G. T. Beckham, C. W. Johnson, E. M. Karp, D. Salvachúa, D. R. Vardon, Opportunities and challenges in biological lignin valorization. *Current Opinion in Biotechnology* **42**, 40-53 (2016).
47. A. J. Ragauskas *et al.*, Lignin Valorization: Improving Lignin Processing in the Biorefinery. *Science* **344**, 1246843 (2014).

48. F. Koopman, N. Wierckx, J. H. d. Winde, H. J. Ruijssenaars, Identification and characterization of the furfural and 5-(hydroxymethyl)furfural degradation pathways of *Cupriavidus basilensis* HMF14. *Proceedings of the National Academy of Sciences* **107**, 4919-4924 (2010).
49. P. Liu *et al.*, Valorization of *Gelidium amansii* for dual production of D-galactonic acid and 5-hydroxymethyl-2-furancarboxylic acid by chemo-biological approach. *Microbial Cell Factories* **19**, 104 (2020).
50. Y.-H. Yang *et al.*, Optimization of growth media components for polyhydroxyalkanoate (PHA) production from organic acids by *Ralstonia eutropha*. *Applied Microbiology and Biotechnology* **87**, 2037-2045 (2010).
51. A. Sydow, T. Krieg, R. Ulber, D. Holtmann, Growth medium and electrolyte-How to combine the different requirements on the reaction solution in bioelectrochemical systems using *Cupriavidus necator*. *Eng Life Sci* **17**, 781-791 (2017).
52. C. Dehio, M. Meyer, Maintenance of broad-host-range incompatibility group P and group Q plasmids and transposition of Tn5 in *Bartonella henselae* following conjugal plasmid transfer from *Escherichia coli*. *Journal of Bacteriology* **179**, 538-540 (1997).
53. F. Kracke *et al.*, Robust and biocompatible catalysts for efficient hydrogen-driven microbial electrosynthesis. *Communications Chemistry* **2**, 45 (2019).
54. F. Kracke, J. S. Deutzmann, W. Gu, A. M. Spormann, *In situ* electrochemical H_2 production for efficient and stable power-to-gas electromethanogenesis. *Green Chemistry* **22**, 6194-6203 (2020).
55. S. T. Lohner, J. S. Deutzmann, B. E. Logan, J. Leigh, A. M. Spormann, Hydrogenase-independent uptake and metabolism of electrons by the archaeon *Methanococcus maripaludis*. *The ISME Journal* **8**, 1673-1681 (2014).
56. J. Myung *et al.*, Long-term cultivation of a stable *Methylocystis*-dominated methanotrophic enrichment enabling tailored production of poly(3-hydroxybutyrate-co-3-hydroxyvalerate). *Bioresource Technology* **198**, 811-818 (2015).
57. N. J. H. Averesch, F. Kracke, Metabolic Network Analysis of Microbial Methane Utilization for Biomass Formation and Upgrading to Bio-Fuels. *Frontiers in Energy Research* **6** (2018).
58. P. Unrean, K. L. Tee, T. S. Wong, Metabolic pathway analysis for *in silico* design of efficient autotrophic production of advanced biofuels. *Bioresources and Bioprocessing* **6**, 49 (2019).
59. R. Cramm, Genomic View of Energy Metabolism in *Ralstonia eutropha* H16. *Microbial Physiology* **16**, 38-52 (2009).
60. M. Kanehisa, S. Goto, KEGG: Kyoto Encyclopedia of Genes and Genomes. *Nucleic Acids Res* **28**, 27-30 (2000).
61. H. Ogata *et al.*, KEGG: Kyoto Encyclopedia of Genes and Genomes. *Nucleic Acids Res* **27**, 29-34 (1999).
62. A. Flamholz, E. Noor, A. Bar-Even, R. Milo, eQuilibrator—the biochemical thermodynamics calculator. *Nucleic Acids Res* **40**, D770-D775 (2011).
63. J. B. van Klinken, K. Willems van Dijk, FluxModeCalculator: an efficient tool for large-scale flux mode computation. *Bioinformatics* **32**, 1265-1266 (2015).
64. I. Vassilev, N. J. H. Averesch, P. Ledezma, M. Kokko, Anodic electro-fermentation: Empowering anaerobic production processes via anodic respiration. *Biotechnology Advances* **48**, 107728 (2021).

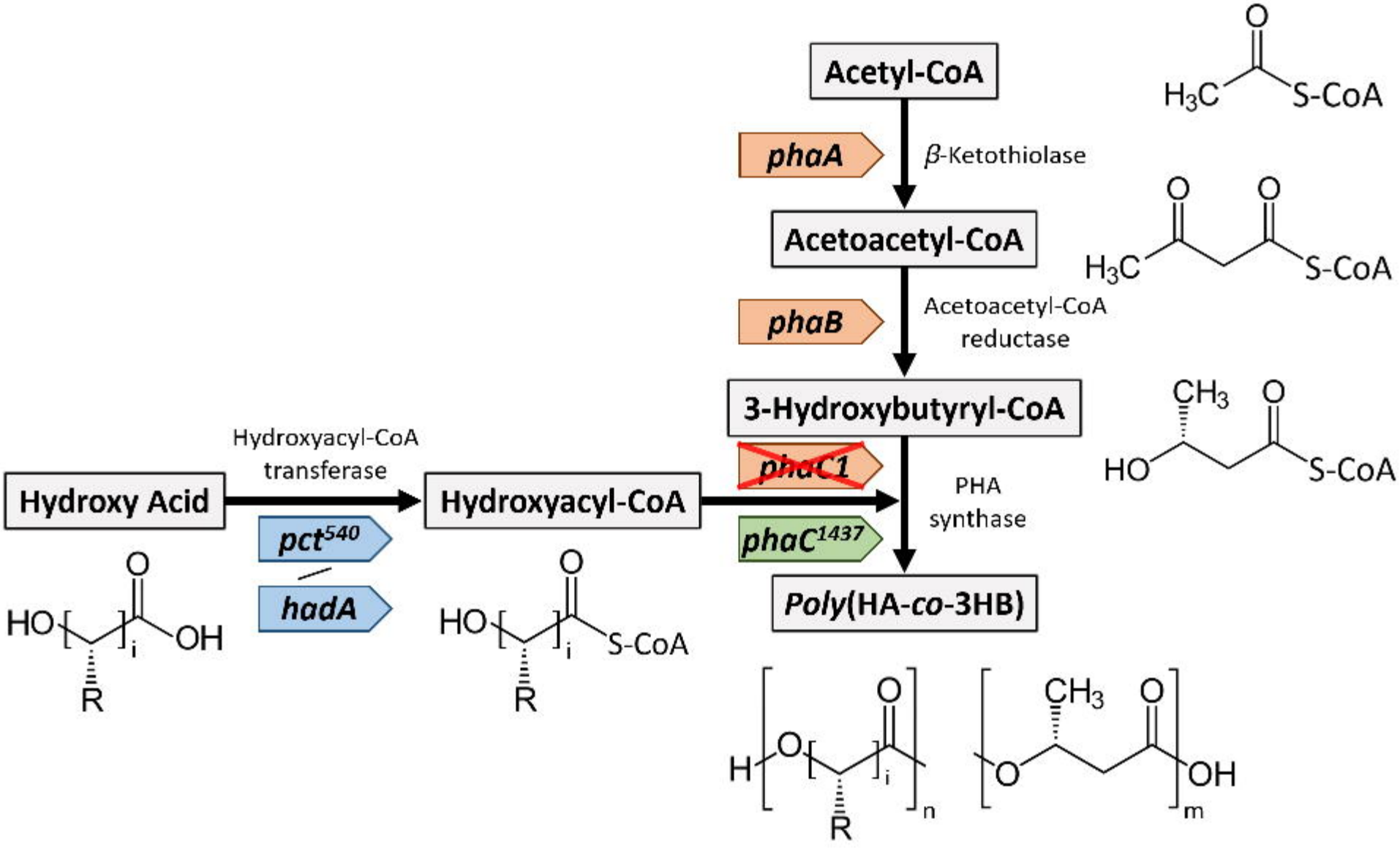

Acetyl-CoA
phaA
β-Ketothiolase
Acetoacetyl-CoA
phaB
Acetoacetyl-CoA reductase
3-Hydroxybutyryl-CoA
phaC1
PHA synthase
phaC1437
Poly(HA-co-3HB)
Hydroxy Acid
Hydroxyacyl-CoA transferase
pct540
hadA
Hydroxyacyl-CoA

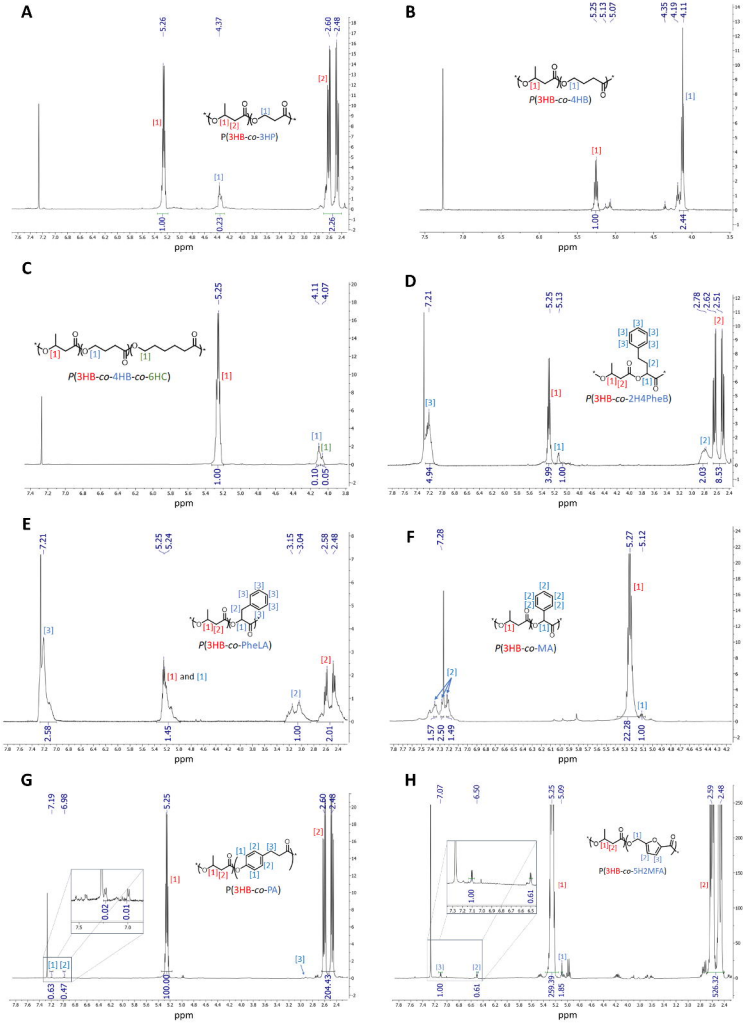
A
5.26
4.37
2.60
2.48
P(3HB-co-3HP)
1.00
0.23
2.26
ppm
B
5.25
5.13
5.07
4.35
4.19
4.11
P(3HB-co-4HB)
1.00
2.44
ppm
C
5.25
4.11
4.07
P(3HB-co-4HB-co-6HC)
1.00
0.10
0.05
ppm
D
7.21
5.25
5.13
2.78
2.62
2.51
P(3HB-co-2H4PheB)
4.94
3.99
1.00
2.03
8.53
ppm
E
7.21
5.25
5.24
3.15
3.04
2.58
2.48
P(3HB-co-PheLA)
[1] and [1]
2.58
1.45
1.00
2.01
ppm
F
7.28
5.27
5.12
P(3HB-co-MA)
1.57
1.53
1.49
22.28
1.00
ppm
G
7.19
6.98
5.25
2.60
2.48
P(3HB-co-PA)
0.02
0.01
0.63
0.47
100.00
204.43
ppm
H
7.07
6.50
5.25
5.09
2.59
2.48
P(3HB-co-5H2MFA)
1.00
0.61
1.08
0.61
299.99
1.88
326.32
ppm

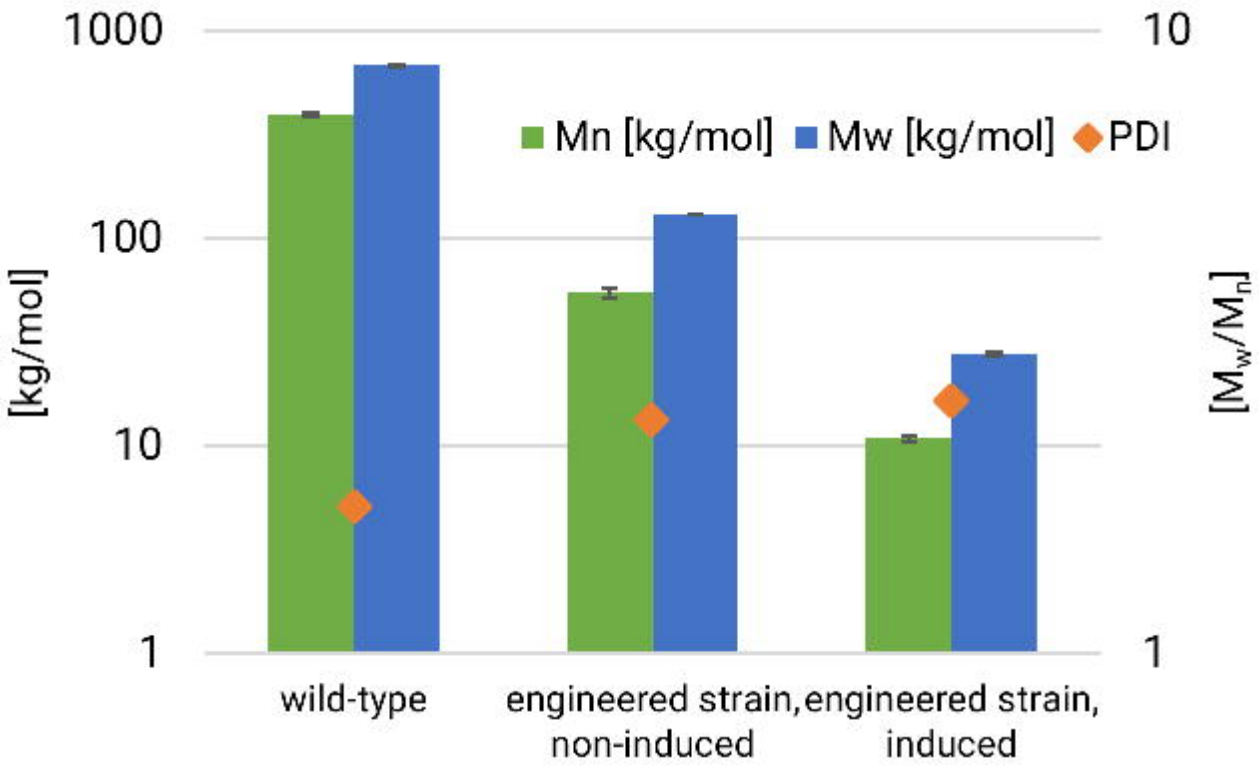
1000
100
10
1
[kg/mol]
10
1
[Mw/Mn]
Mn [kg/mol]
Mw [kg/mol]
PDI
wild-type
engineered strain, non-induced
engineered strain, induced

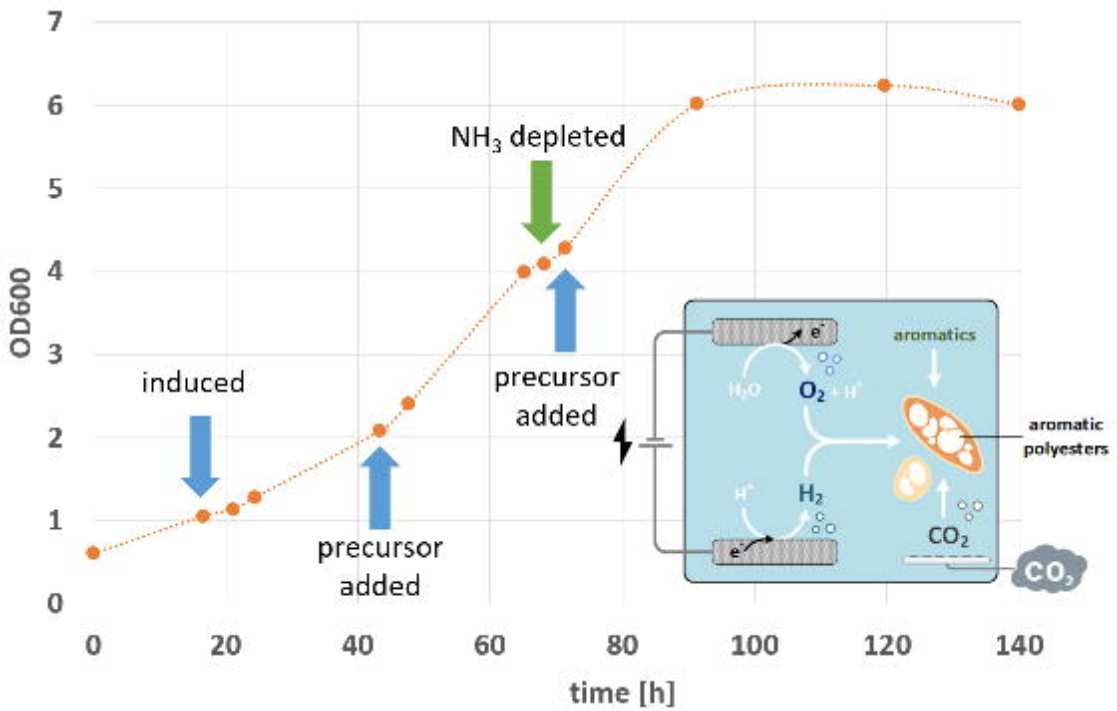
OD600
time [h]
induced
precursor added
NH3 depleted
precursor added
aromatics
aromatic polyesters
H2O
O2 + H+
H+
H2
CO2
CO2
e-
e-